1-D velocity structure modelling of the Earth's Crust in the NW Dinarides

Gregor Rajh[1], Josip Stipčević[2], Mladen Živčić[3], Marijan Herak[2], Andrej Gosar[1,3], and the AlpArray Working Group[+]

[1]University of Ljubljana, Faculty of Natural Sciences and Engineering, Ljubljana, Slovenia
[2]University of Zagreb, Faculty of Science, Geophysics Department, Zagreb, Croatia
[3]Slovenian Environment Agency, Seismology Office, Ljubljana, Slovenia
[+]The complete member list of the AlpArray Working Group is at the end of the paper.

Correspondence to: Gregor Rajh (gregor.rajh@ntf.uni-lj.si)

Abstract. The investigated area of the NW Dinarides is located at the NE corner of the Adriatic microplate and is bordered by the Adriatic foreland, the Southern Alps, and the Pannonian basin. Its complex crustal structure is the result of interactions among different tectonic units, mainly the Eurasian plate and the Adriatic microplate. Despite numerous seismic studies in this tectonically complex area, there is still a need for a detailed, small scale study focusing mainly on the upper, brittle part of the crust. We investigated the crustal velocity structure with 1-D simultaneous hypocenter-velocity inversion using routinely picked P wave arrival times. Most of the computed models converged to a stable solution in the depth range between 0 and 26 km. We further evaluated the inversion results with hypocenter shift tests, high and low velocity tests, and relocations. This helped us to select two best performing velocity models for the whole study area. Based on these results and the seismicity distribution, we further divided the study area into three parts, redefined the earthquake-station geometry, and performed inversion for each part separately to gain better insight into the crustal structure of each subregion. Median velocities in the upper 20 km of the crust in the eastern subregion are lower compared to the regional median and the median of the other two subregions. The northwestern and southwestern subregions are very similar in terms of crustal structure between about 8 and 23 km depth. The largest difference between them is observed in the upper 8 km, with higher median velocities in the southwestern subregion. Compared to the model currently used at Slovenian Environment Agency to locate earthquakes, the velocity models obtained show higher velocities in the upper 30 km depth and agree very well with some of the previous studies. In addition to general structural implications and a potential for improving seismic tomography results, the new 1-D velocity models can also be used for fast routine earthquake location and for detecting systematic travel time errors in seismological bulletins.

1 Introduction

The study area of the NW Dinarides lies at the northeastern corner of the Adriatic microplate and is bounded to the north by the Southern Alps, to the east by the Pannonian basin, and to the west by the Adriatic foreland, thus representing an

important junction between these units (Fig. 1). The evolution of the Dinarides is tied to the ongoing collision between the Eurasian plate (Eurasia) and the Adriatic microplate (Adria), which began in the late Cretaceous (Tari, 2002; Handy et al., 2010; Ustaszewski et al., 2010; Handy et al., 2015).
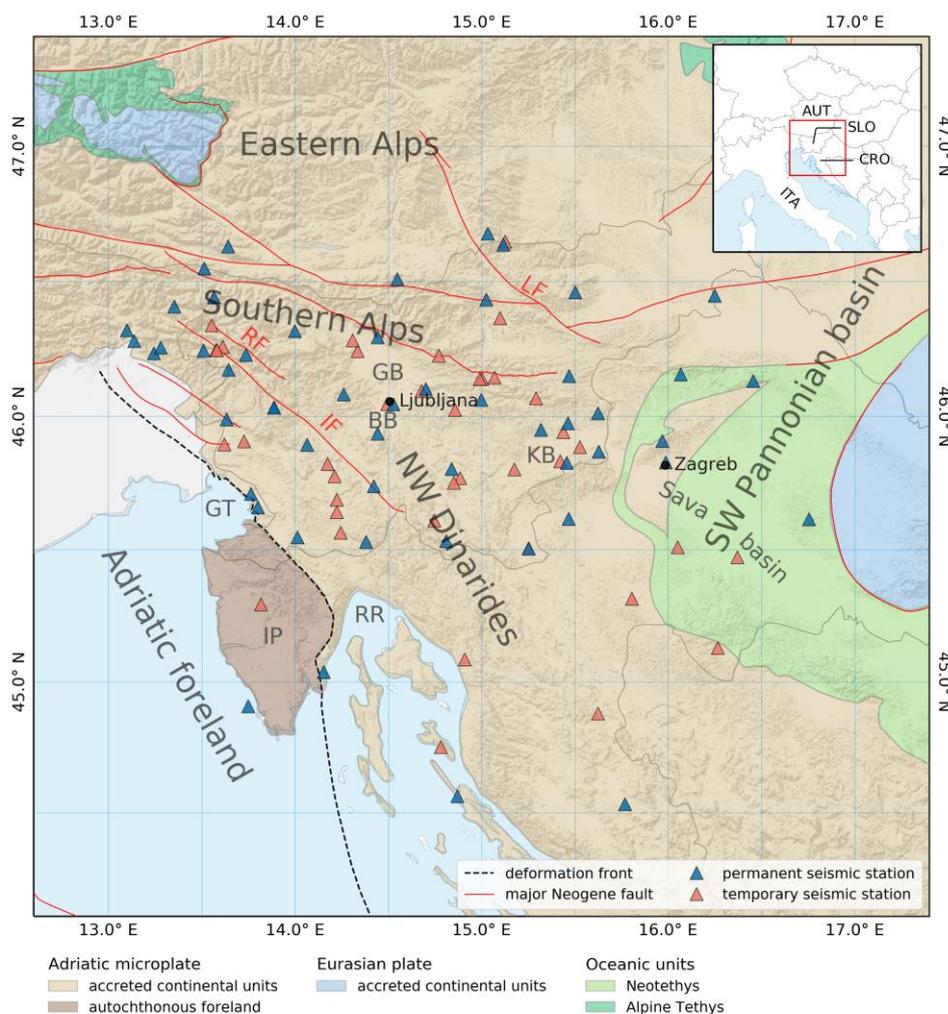
Figure 1: Map of the study area. Seismic stations used in this study are shown on top of the regional tectonic map and major Neogene faults (adapted from Schmid et al., 2008). Black dashed line represents the current main deformation front of the Dinarides. GT, Gulf of Trieste; IP, Istra peninsula; RR, Rijeka region; GB, Gorenjska basin; BB, Barje basin; KB, Krško basin; IF, Idrija fault; RF, Ravne fault; LF, Labot fault; AUT, Austria; CRO, Croatia; ITA, Italy; SLO, Slovenia. Shaded relief is shown
40 **in the background (Esri, USGS, NOAA).**

First 3-D compressional (P) wave velocity model in this area was obtained with local earthquake tomography (LET) study done by Michelini et al. (1998). It revealed two areas of distinct high and low velocities in western and eastern Slovenia,

which were interpreted as the upper crustal expression of the ongoing convergence between the Adria and the Eurasia. The authors also proposed a relocation study using the 3-D velocity model to map active faults and trends in seismicity. This was partly realised by a study that focused on the Idrija fault system in western Slovenia (Vičič et al., 2019). Its authors were able to constrain the geometry of each fault by relocating microseismicity with the regional 3-D shear (S) wave velocity model of Guidarelli el al. (2017) and a constant *Vp/Vs* value. The model of Guidarelli et al. (2017) was obtained with ambient seismic noise tomography and shows distinct lateral change in the crustal structure under western Slovenia. This was interpreted as a transformation from a uniform to a more variable crustal structure across the bounding strike-slip Idrija fault, indicating transition between the Dinarides and the Pannonian basin units. Recently, Kapuralić et al. (2019) computed a 3-D P wave velocity model from LET and used these results to constrain the relationship between the crust and the uppermost mantle at the junction between the Dinarides and the Pannonian basin. Their findings show significant changes in the crustal structure at the transition zone between the NW Dinarides and the Pannonian basin and map several zones of higher seismic velocity in the NW Dinarides crust. As opposed to the model of Guidarelli et al. (2017), this 3-D velocity model shows no obvious crustal signature of the dividing Idrija fault. Direct comparison between P and S wave velocity models should be done with care due to the highly variable average *Vp/Vs* values in the region (Behm, 2009; Stipčević et al., 2020). The latest receiver functions study applied to the Dinarides and the surrounding area (Stipčević et al., 2020) showed the transition from the thick Dinaric to the thinner Pannonian crust, and indicated that the depth of earthquakes generally follows the shape of the Mohorovičić discontinuity (Moho). Surface wave dispersion study in Slovenia by Živčić et al. (2000) showed a 4-6 km thick layer with S wave velocities between 2.75 and 3.00 km s^{-1} above of a 7-9 km thick layer with S wave velocities between 3.00 and 3.30 km s^{-1}. The velocity of the underlying layer was found to be lower in eastern Slovenia. Their results also suggest comparatively higher velocities deeper in the upper crust in western Slovenia.

Despite the numerous investigations that covered the study area, the details of the upper crustal structure remained unresolved. Moreover, the 3-D velocity models covering the study area show markedly different and rapid lateral velocity variations in the upper crust. For these reasons, there is still a need for a detailed, small scale study focusing mainly on the upper, brittle part of the crust. Therefore, our goal is to investigate the velocity structure of the crust using the concept of a minimum one-dimensional (1-D) velocity model. The minimum 1-D velocity model is computed by simultaneous inversion for hypocenter and velocity parameters (coupled hypocenter-velocity problem) and represents the best fit to the observed travel time data in the least-squares sense. This iterative approach is necessary because of the strong coupling between hypocenter and velocity parameters (Kissling, 1988; Kissling et al., 1994). If obtained properly, the minimum 1-D velocity model can be used to calculate accurate earthquake locations (e.g., Husen et al., 1999) and to detect systematic errors in travel time data (e.g., Maurer et al., 2010), especially when computed at a smaller scale (Husen et al., 2011). Station delays computed as part of the minimum 1-D velocity model allow identification of major geological and tectonic features or trends. The minimum 1-D velocity model is also essential for 3-D velocity modelling in LET, where it is commonly used as an initial model in inversion (e.g., Kissling, 1988; Kissling et al., 1994; Haslinger et al., 1999; Diehl et al., 2009). Using a

minimum 1-D velocity model as the initial model in LET can greatly reduce inversion artefacts in a final 3-D velocity model and improve error estimates (Kissling et al., 1994).

80

Most of the seismicity in the study area has been located with the synthetic 1-D velocity model (routinely used 1-D velocity model, R1D from now on) aggregated mainly from the results of Michelini et al. (1998) and Živčić et al. (2000). Compared to today's situation, the results of these studies were obtained with a relatively small amount of data. Seismic station coverage in the area improved significantly with the gradual modernization of the Seismic network of the Republic of Slovenia (SNRS) between 2001 and 2008 (Jesenko & Živčić, 2018) and the deployment of additional seismic stations in Croatia within the VELEBIT project (2015-2019), and during 2015 and 2016 as part of the AlpArray project (Molinari et al., 2016). With better station coverage and smaller epicentral distances, we are now able to sample the upper crustal structure more densely, and therefore calculate more accurate upper-crustal velocity models. Furthermore, studying spatial distribution of the relocated seismicity allows us to put additional constraints on the crustal structure and the processes driving the seismicity itself.

90

2 Tectonic setting and crustal structure

The tectonic evolution of the study area is closely related to the dynamics of the Adria. The subduction processes associated with the closure of the Neotethys ocean started in the Jurassic (Pamić et al., 1998; Tari, 2002; Schmid et al., 2008) and led to the continental collision between the Adria, which at that time detached from the African plate (Schmid et al., 2008), and the Eurasia in the late Cretaceous (Tari, 2002; Handy et al., 2010; Ustaszewski et al., 2010; Handy et al., 2015). The collisional processes that occurred along the northern (e.g., Kissling et al., 2006) and western (e.g., Vignaroli et al., 2008) margins of the Adria, gave rise to the Alps and the Apennines, respectively. Along the eastern margin, the collisional process started after the oceanic part of the Adria was consumed in the subduction, leading to the formation of the thrust sheets and the ophiolitic units of the Neotethys (Schmid et al., 2008). The subduction ceased in the early Paleogene (Pamić et al., 1998; Schmid et al., 2008) and the deformation front began to migrate southwestward (Tari, 2002; Korbar, 2009; Ustaszewski et al., 2010; Handy et al., 2015). The peak of this ongoing deformation event lasted until the early Oligocene and was expressed by the foreland directed thrusting (Pamić et al., 1998; Tari, 2002; Schmid et al., 2008; Placer et al., 2010), which strongly deformed the upper crust of the Adria (Schmid et al., 2008; Korbar, 2009). At the same time, the continental part of the Adria began to underthrust the Dinarides (Tari, 2002; Placer et al., 2010). In addition, the movement of the Adria was responsible for the late Oligocene-Miocene south verging thrusting in the Southern Alps (Schmid et al., 2004; Handy et al., 2010; Handy et al., 2015) and the lateral extrusion of the Eastern Alps. Major contributing factor for the lateral extrusion of the Eastern Alps was the extension of the area behind the retreating subduction zone in the Carpathians (Ratschbacher, 1991a, 1991b; Horváth & Cloetingh, 1996), which led to the formation of the Pannonian basin. In the late Miocene, the onset of counterclockwise rotation of the Adria (Márton et al., 2003; Márton, 2006) and the termination of the subduction in the

110 Carpathians (Horváth & Cloetingh, 1996) led to transpressive reactivation of the of the former extensional structures in the Pannonian basin (Horváth & Cloetingh, 1996; Fodor et al., 1999; Tari, 2002, Ustaszewski et al., 2010) and transpressive to pure strike-slip deformation along the zone of steep, NW-SE striking faults in the Dinarides and the Southern Alps (Picha, 2002; Placer et al., 2010; Vičič et al., 2019).

115 Crustal thickness in the NW Dinarides, has been recently constrained by many different studies (Brückl et al., 2007; Behm et al., 2007; Šumanovac, 2010; Stipčević et al., 2011; Guidarelli et al., 2017, Kapuralić et al., 2019; Stipčević et al., 2020). It varies from about 38 to 45 km under the External Dinarides, slightly thickening towards the Alps and thinning to about 30 km in the Adriatic foreland and 25 km in the Pannonian basin. A similar pattern was observed for the lithosphere thickness in the same area (Belinić et al., 2018). The underthrusting of the Adria under the External Dinarides resulted in two-layered 120 and thickened crust under the External Dinarides. The thinner crust in the Adriatic foreland is associated with the undeformed parts of the Adria. The extension in the late Oligocene and early Miocene, which caused crustal thinning in the Pannonian basin, is most likely responsible for relatively low seismic velocities in the upper and middle crust under the transition zone from the Southern Alps and the Dinarides to the Pannonian basin. The thinned crust that comes into contact with the Adria in this transition zone belongs to the Pannonian fragment. The junction between these two units appears as a 125 10 km jump in Moho depth, probably a result of the crustal thinning. The ongoing convergence between the Adria and the Eurasia could be compensated here by underthrusting of the Adriatic mantle under the Pannonian mantle (Brückl et al., 2007; Brückl et al., 2010).

Throughout the study area the seismicity is mostly constrained to the upper crust (Herak et al., 1996, Slovenian Environment 130 Agency, 2019). Several strong historical and instrumentally recorded earthquakes occurred in this region. The strongest historical earthquake with estimated magnitude of about M_W=6.8 and a maximum estimated intensity of X EMS-98 occurred in 1511 on the Idrija fault in western Slovenia (Vidrih & Ribičič, 2004; Fitzko et al., 2005; Cecić & Jocif, 2011). The Rijeka region was hit by four damaging earthquakes between 1750 and 1904 with maximum intensity estimates from VI to VIII MSK (Herak et al., 2017; Herak et al., 2018). The strongest historical earthquake near Zagreb occurred in 1880 with a 135 maximum intensity of VIII MCS (Herak et al., 1996). Shortly after, two destructive earthquakes occurred in Slovenia. In 1895, an earthquake near Ljubljana (central Slovenia) occurred with M_W 6.0 (VIII-IX EMS-98) (Lapajne, 1989; Tiberi et al., 2018) and in 1917, an earthquake with M_W 5.6 (VIII EMS-98) struck the Krško basin (Lapajne, 1989; Cecić et al., 2018). Recently, two strong earthquakes occurred on the Ravne fault in northwestern Slovenia. The first in 1998 with M_W 5.6 and a maximum intensity of VII-VIII EMS-98 (Zupančič et al., 2001) was followed by an earthquake with M_W 5.2 (VII EMS-98) 140 in 2004 (Vidrih & Ribičič, 2004). The most recent damaging events in this area occurred in Croatia near Zagreb (M_W 5.3; GEOFON, 2021) and Petrinja (M_W 6.4, GEOFON, 2021) in 2020.

3 Data

The seismological bulletin (Slovenian Environment Agency), consisting of 7,733 local earthquakes with M_L of at least 1.0 that occurred between 2004 and 2018, served as a starting point for this study. The earthquakes are routinely analysed by the

145   Slovenian Environment Agency (ARSO) and cover the entire territory of Slovenia and its surroundings. Their locations were determined with the HYPOCENTER program (Lienert & Havskov, 1995) using P and S arrival times and the routine 1-D velocity model. Blasts and explosions are removed from the main catalogue and are used as an independent data set for testing. The arrival times in the seismological bulletin were grouped into six uncertainty classes based on uncertainty intervals subjectively determined by the analysts, as shown in Table S1. The best estimated first P arrival times (classes 0, 1,

150   2) dominate in our data set and there are only a small number of arrival times within uncertainty classes 3 and 4. For our study, we kept only the arrival times belonging to uncertainty classes 0, 1, and 2.

Most earthquakes in the study area are confined to depths between 1.1 km and 18.3 km (5th and 95th percentiles). The strongest earthquake in our data set had a M_L 4.9 and is one of the few earthquakes that exceeded M_L 4.0. Earthquakes of the

155   lowest magnitude considered (M_L 1.0) had on average 9 P and 8 S arrival time picks, which is sufficient for a good location estimate. Moreover, the arrival times of these smaller earthquakes were still reliably picked (uncertainty class $\leq$ 2) at maximum average epicentral distance of about 84 km.

The study area is densely populated with seismic stations (Fig. 1). The arrival times were picked mainly at seismic stations

160   of the Seismic Network of the Republic of Slovenia (Slovenian Environment Agency, 2001) together with seismic stations belonging to other seismic networks and temporary seismic arrays in the region (Zentralanstalt Für Meteorologie Und Geodynamik, 1987; MedNet Project Partner Institutions, 1990; University of Zagreb, 2001; OGS, 2002; INGV Seismological Data Centre, 2006; AlpArray Seismic Network, 2015; OGS, 2016). The Seismic Network of the Republic of Slovenia (SNRS) was gradually modernised between 2001 and 2008 and currently consists of 26 permanent stations (Vidrih

165   et al., 2006; Jesenko & Živčić, 2018). During the last 16 years, many temporary stations have been in operation in Slovenia. Some additional seismic stations were also deployed in Croatia in recent years as part of the VELEBIT project and the AlpArray project (Molinari et al., 2016). These stations mostly filled the gaps between the permanent stations of the Croatian Seismic Network (CR). Some seismic stations located in Austria and Italy were used to better cover the periphery of our study area.

170   ## 4 Method

Observations of seismic phase arrival times can be used to investigate seismic velocity structure of Earth's interior. Arrival time of a wave (T_{ij}) generated by an earthquake (i) and observed at a station (j) is a nonlinear function of station coordinates (s_j), hypocenter parameters (h_i), and velocity model parameters (m). This function can be approximated with a Taylor series

expansion about the points in a hypocenter and a velocity model solution space (h_i^0, m^0). By only keeping linear terms we

175 obtain its linearised form

$$T_{ij} = T_{ij}^0 + \sum_{k=1}^{4} \left[\frac{\partial T_{ij}}{\partial h_{ki}}\right]_{h_i^0, m^0} \Delta h_{ki} + \sum_{k=1}^{p} \left[\frac{\partial T_{ij}}{\partial m_k}\right]_{h_i^0, m^0} \Delta m_k + e \ , \tag{1}$$

which relates small changes in arrival time to small changes in the hypocenter and the velocity model parameters. The third

term is summed over the total number of velocity model parameters (p). The error term (e) contains arrival time errors

caused by the approximation and errors in calculated and observed arrival times.

180

By estimating (predicting) hypocenter and velocity model parameters, we can calculate arrival time (T_{ij}^0) of an earthquake

phase, and all partial derivatives in Eq. 1. We do this numerically by tracing rays for predicted hypocenter parameters

through predicted velocity structure (e.g., Crosson, 1976; Kissling, 1988). The difference between the calculated and

observed arrival time can be expressed as an arrival or travel time residual, which is related to the perturbations (corrections)

185 in the hypocenter and velocity model parameters, Δh_{ki} and Δm_k, respectively. For I earthquakes, each observed at J stations,

we obtain a system of $N = I$ x J linear equations, which we solve by minimizing the misfit (residual) to the data with the

damped least squares approach (e.g., Crosson, 1976; Aki et al., 1977; Kissling, 1988). Because we are solving

simultaneously for hypocenter and velocity parameters, this inverse problem is known as the coupled hypocenter-velocity

problem. Since the system of equations which we are solving is not a true linear system, the hypocenter and velocity model

190 perturbations must be small. Therefore, an initial estimate of the unknown parameters must be sufficiently close to the

correct solution and the inversion performed iteratively by adjusting hypocenter and velocity model parameters in each step

(Crosson, 1976).

The result of the coupled hypocenter-velocity problem described above is the velocity model (velocities and possibly station

195 delays) and the revised hypocenter parameters. The resulting model minimizes the travel time residuals and is referred to as

the minimum 1-D velocity model in the case of the 1-D parameterization. The 1-D model approaches the average of the 3-D

velocity model blocks, weighted by the total ray length in each block. In other words, the layer velocities of a 1-D velocity

model approximate the average velocity of a 3-D velocity model in the same depth interval. The construction of a minimum

1-D model is a trial-and-error process that requires careful selection of only high-quality data and rigorous evaluation of the

200 results (Kissling et al., 1994).

5 1-D velocity modelling

5.1 Initial data set

To sufficiently sample the solution space, several different initial 1-D velocity models (Fig. 2) were used as input to the inversion. Among them, three initial models (a priori initial models) were derived from the independent studies (Brückl et
205 al., 2007; Šumanovac, 2010) and from the synthetic 1-D velocity model routinely used at ARSO to locate earthquakes (R1D). Two initial models with low and high velocity values were also included in the inversion procedure. They were subjectively defined to roughly envelop the lowest and highest velocity values of the a priori models with an average buffer of about 0.15 km s^{-1}, while keeping the inversion stable. Using several different models allowed us to better sample the solution space and test the dependence of our solution on an initial model. To define the layered structure, we started with
210 thicker layers and thinned them at more densely sampled depth intervals, paying close attention to the change in the RMS residual and the convergence of the models. The differences between the adjacent layers were kept as small as possible to ensure stability during the inversion. The surface layer (above 0 km) is used to trace the rays all the way to the station elevation and usually shows coupling with the station delays.
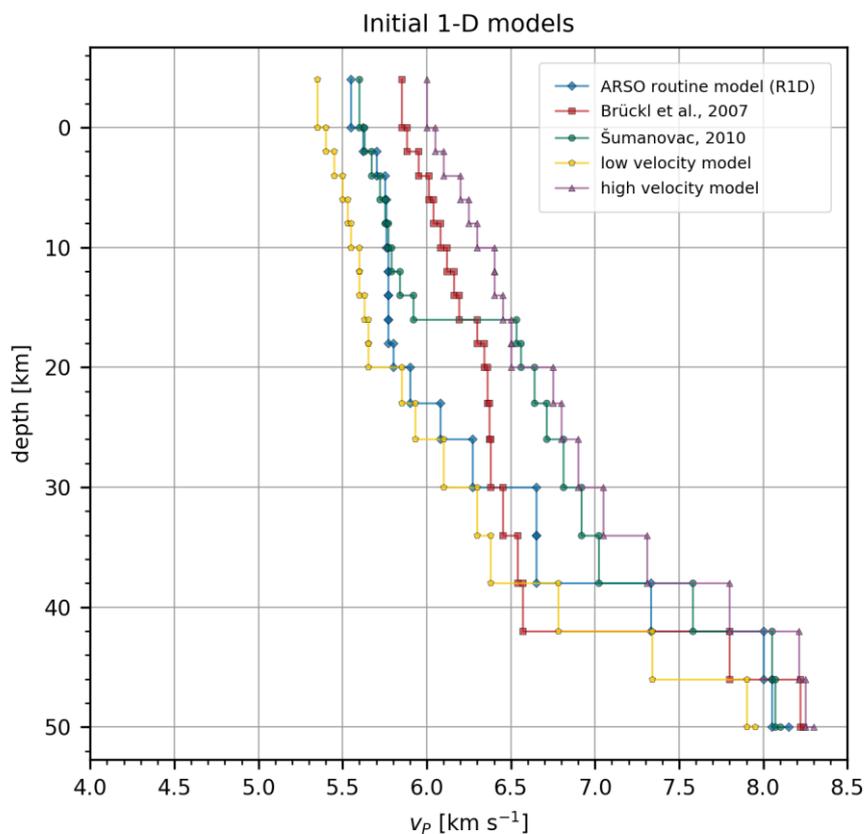
215 **Figure 2:** **Initial 1-D models constructed from a priori data (blue, red, green). Low velocity model (yellow) and high velocity model (violet) roughly envelop all a priori models and are used to further sample the solution space.**

The aim of the earthquake selection procedure is to select a high-quality earthquake data set that is uniformly distributed over an investigated volume and has the highest number of quality first arrival time picks. Routinely determined hypocenter parameters were used and we kept only the first P arrival times of the selected seismic stations (Fig. 1 and 4) with uncertainty class of 2 or better. Earthquakes with a depth of 0 km, a maximum azimuthal gap greater than 160°, RMS residual of more than 0.5 s, and fewer than 10 remaining first P arrivals were removed. After several tests, the studied area was tessellated into square cells of 10 km (Fig. 3). For each cell, events were sorted by their parameters and iteratively selected to obtain the most diverse depth distribution possible and avoid clustering. This was achieved by setting the minimum vertical distance between the earthquakes within a single cell to 2 km, a value determined by a trial-and-error approach based on the final number of earthquakes selected. The earthquakes in each cell were hierarchically sorted by (descending in importance) a number of travel times with uncertainty class 0, a number of travel times with uncertainty class 1, a total number of travel times, azimuthal gap, magnitude, and a number of stations with readings. The first earthquake from the sorted list was selected and then the others followed iteratively according to the minimum depth distance.
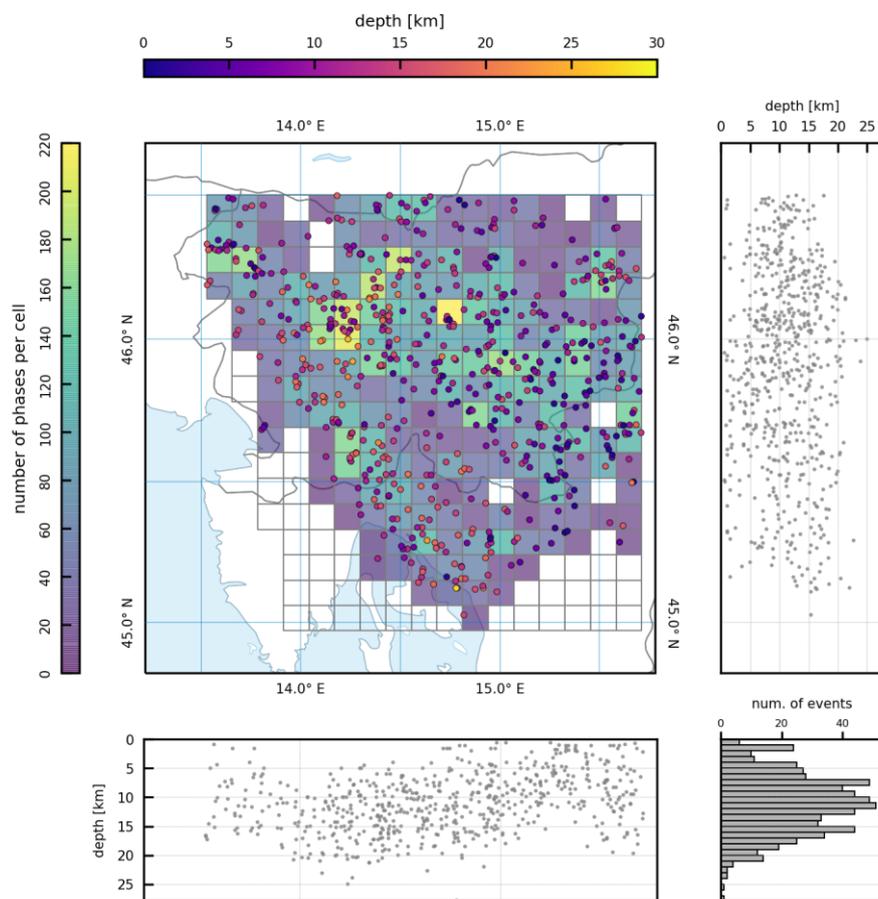
Figure 3: Earthquake data set selected for the inversion. Square 10 km cells shown on the main map were used to select earthquakes. Colour of each cell represents the total number of P phases per cell. The right and bottom panels show the hypocenters of earthquakes projected on N-S and W-E oriented profiles, respectively. The histogram in the lower right corner shows the number of earthquakes in 1 km depth bins for the whole study area.

Using the earthquake selection procedure described above, we obtained a high-quality data set of 631 earthquakes (Fig. 3) and 15,579 readings of first P arrival times with a maximum epicentral distance of 266 km. Of these, 14,677 were manually picked as Pg phases, while 423 were picked as Pn phases. Epicentral ray coverage was determined by connecting earthquake station pairs with great circles and counting rays intersecting 10 km grid cells (Fig. 4). The earthquake selection grid was truncated in places where seismicity is sparse (e.g., Istra peninsula). Its extent was also limited by the spatial extent of the earthquakes in the seismological bulletin. We also made sure that the selected earthquakes were surrounded by seismic stations from all sides.
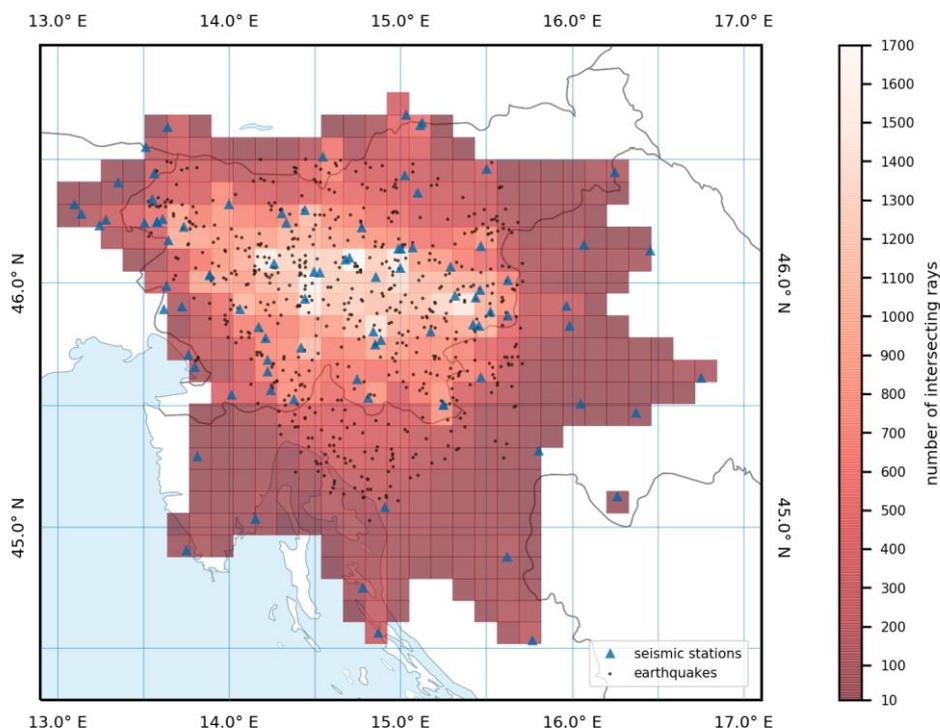
245

Figure 4: Number of great-circle rays intersecting square 10 km grid elements and connecting earthquake-station pairs for the earthquakes shown in Fig. 3. Grid elements with less than 10 intersecting rays are not shown.

5.2 Modelling process

250 To compute 1-D velocity models, we used the VELEST code (Kissling et al., 1994; version 4.5) and followed the guidelines for computing a minimum 1-D velocity model from Kissling et al. (1994), Husen et al. (2011), and the VELEST user manual (Kissling, 1995). The VELEST code has been improved through the efforts of many authors and has become very versatile and robust. It also allows the calculation of station delays, which enter the inversion as unknown velocity model parameters and are thus part of the 1-D velocity model (Kissling, 1988). In general, the computation of a 1-D velocity model was

255 performed in two runs. In the first run, the hypocenter parameters were computed at each iteration, while the velocity model parameters were adjusted along with the hypocenter parameters at every other iteration. This approach was necessary because we performed separate inversion for each initial 1-D velocity model (Fig. 2) with the same set of routinely determined initial hypocenter parameters. We set the damping to 0.01 for the hypocenter parameters and station delays and to 0.10 for the velocity parameters, as suggested by Kissling et al. (1994). In the second run, the hypocenter parameters and

260 velocity model obtained in the first run were used as input, the station delays were set to zero, and all parameters were computed at each iteration. We left the damping for the hypocenter parameters and station delays unchanged but increased

the damping for the velocity parameters to 1.00 (Kissling et al., 1994) and to 10.00 (Husen et al., 2011) in two separate computations. Increasing only the damping of the velocity parameters in the final run prevents large perturbations in the velocities, especially in the poorly sampled layers, but allows for larger ones in the hypocenter parameters and station delays.

265 This, together with the computation of all parameters at each iteration, leads to only fine adjustments close to the previous solution (Husen et al., 2011) and the 1-D velocity model that minimize the total estimated location errors (Kissling et al., 1994).

Iteration in the VELEST is stopped, when the RMS residual or data variance ceases to decrease, or when the predefined

270 number of iterations is reached. Due to lower damping values, different iteration types, and poor sampling in one of the layers, it is also possible that the inversion becomes unstable and has to be stopped prematurely. For this reason, and because some initial models are closer to the final solution than others, the total number of iterations was set between 2 and 8 for the first run. For the second run, the total number of iterations was set to 3, 5 and 7. This also allowed us to examine and test the results of the inversions that diverged during the latter iteration steps. In general, the inversions with the lowest number of

275 iterations were found to be unstable in the tests described below. We did not allow for low-velocity layers in the inversion as this resulted in larger instabilities.

5.3 Tests

To check for any bias and to assess the stability of the solutions, all the obtained 1-D velocity models were subjected to several tests. The obtained hypocenter locations were systematically shifted by 10 km to greater depths and pseudorandomly

280 shifted in by 10 to 15 km in arbitrary direction before being introduced into another inversion run. The damping parameters of this inversion run were identical to those of the second run, but this time we used the input station delays and computed the velocity model at every other iteration out of a total of nine, as suggested by Kissling (1995). If the velocities, station delays, and origin times remained relatively unchanged after this test and the hypocenters were relocated back to their initial positions, a stable solution was obtained and there should be no significant bias in the velocity model that could result from a

285 systematic shift of the hypocenters. We further tested the stability of each velocity model using the so-called high/low tests (Haslinger et al., 1999) by varying the velocities of the obtained models by ±0.5 km s⁻¹ and using them as initial models in an inversion run similar to that of the hypocenter shift test but performing a simultaneous hypocenter-velocity inversion at each iteration. Models with large RMS residuals and large deviations in the velocity model and hypocenter parameters after these tests were not considered suitable candidates for the minimum 1-D velocity model. The models with the lowest RMS

290 residuals also performed well in the tests, implying that RMS residual can be used as the first quality indicator for a 1-D velocity model. The tests can also be used to assess the coupling between the hypocenter and the velocity model parameters.

To see which obtained velocity models and station delays yield reasonable hypocenter locations, we relocated all well-locatable earthquakes (maximum azimuthal gap of 180° and at least 10 first P arrival times with uncertainty class less than 3)

295 with each obtained 1-D velocity model. The quality of each solution was also evaluated by relocating blasts with known location and comparing the calculated station delays with the a priori knowledge of the geological structure in the region. Together with the hypocenter shift tests, relocation of blasts can provide an approximate estimate of the absolute uncertainty of the hypocenter location (Haslinger et al., 1999). Because hypocenter locations can be systematically shifted toward the surface due to an inappropriate velocity model, relocation of blasts can give the false impression of a very good depth

300 estimate. Therefore, the performance of an individual model should not be judged solely based on relocation of blasts. By observing the consistent patterns of relocated blasts among different models, one can also evaluate the performance of a seismic network for locating earthquakes in different parts of a study area.

6 Results

Throughout the modelling process, many 1-D velocity models were obtained from different initial 1-D velocity models and
305 inversion parameters. We focus only on the results obtained from the a priori initial models (R1D; Brückl et al., 2007; Šumanovac, 2010) shown in Fig. 2 and note that the models obtained from the initial models with low and high velocities converged partially towards the solution obtained with the a priori initial models and performed comparatively poorly in the tests. This suggests that it is very difficult to obtain a stable solution when the starting point in the parameter space is relatively far from the true model. Nevertheless, these results serve as another indicator of how well the velocity in each
310 layer is constrained.

Using only the a priori initial models, 36 velocity models (final models; Fig. S2) were obtained with different total number of iterations and with a damping value for the velocity parameters in the second run set to 10.0. With this damping value, we obtained better convergence and slightly lower RMS residuals, but in practice no large difference was observed in well-
315 sampled layers when it was set to 1.0. The final models show very good convergence for layers between 4 and 34 km (Fig. 5 and S2, Table S3). The topmost layers and layers below 38 km remained more or less unconstrained. The final RMS residuals for the inversion data set are mostly below 0.240 s, with the lowest value of about 0.225 s (Fig. S4), and generally show a reduction of up to 20-33 percent compared to the first iteration. Based on the RMS residuals, stability tests, and relocations, two (minimum) 1-D velocity models were selected. These models have very similar velocities, same general
320 pattern of station delays, and are also very close to the median velocities calculated from all final models (Fig. 5). They were both computed from the R1D velocity model, but with different number of iterations in each run. For brevity, we show detailed results only for the model that performed marginally better in the tests.
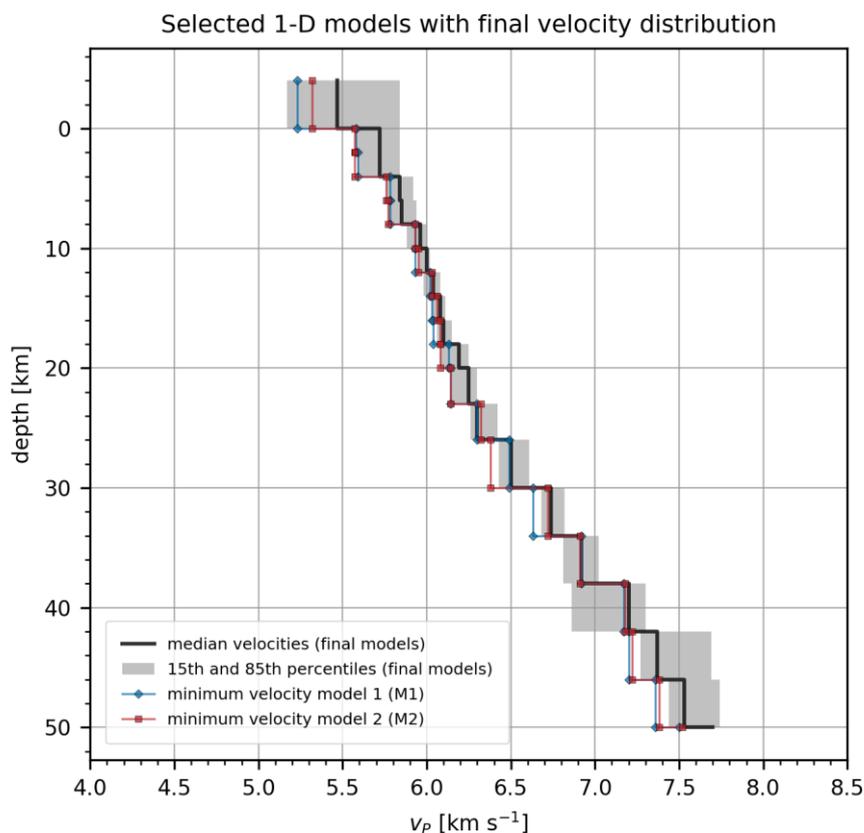
Figure 5: Two selected velocity models (blue, red) chosen after examining the results of stability tests, relocations, and final RMS residual values. Also shown are the median velocities (black line) and velocity percentiles (grey area) of final models as calculated in each layer and obtained from the a priori initial models. Corresponding values are given in Table S3.

6.1 Example for the minimum velocity model 2

The minimum velocity model 2 (M2) was computed from the R1D model with six total iterations in the first run and five total iterations in the second run. It shows a gradual increase in the velocities from 5.57 km s⁻¹ at 0 km depth to 6.38 km s⁻¹ at 26 km depth (Fig. 5). At 30 km depth, we observe a jump in velocity to 6.72 km s⁻¹. While this jump in velocity is less pronounced in the other minimum model, it already appears at 26 km depth. Less than 900 rays penetrated the layers between 26 and 42 km depth, which were sampled in only a few directions because earthquakes in the study area occur only at shallower depths (Fig. 6). This prevents us from better constraining the velocities in these layers. The layers below 42 km were sampled with only eight rays, which means that the velocities at these depths remained unconstrained. The computed station delays show the same general trend for all final models and were referenced to the seismic station with many high-quality picks and a location approximately in the middle of the selected seismic stations (Fig. 7). Seismic stations in the west

show large negative delays that gradually transition to more positive delays in the east and southwest. We observe relatively
340   large positive station delays in the Krško basin, Sava basin and in other sedimentary basins such as the Barje and Gorenjska
basins. Slightly negative station delays appear in the region of magmatic and metamorphic rocks in the Eastern Alps
(northeast of the Labot fault). In the southern part of the study area, we observe another zone of positive station delays
extending approximately in the NW-SE direction along the Adriatic coast, starting at the Istra peninsula. Less pronounced
negative station delays from the northwest seem to extend to the south in the same direction but more inland. This trend is
345   interrupted by the southernmost seismic station (UDBI), which shows positive station delay. Deeper and large-scale velocity
variations in the crust are reflected more on the delays of seismic stations with limited azimuthal coverage at the periphery of
the study area. This is mainly because of longer ray paths that travel mostly through the poorly sampled parts of the crust
away from the volume sampled by most of the rays (Fig. 6). Refer to Fig. 1 for all mentioned geographical locations.
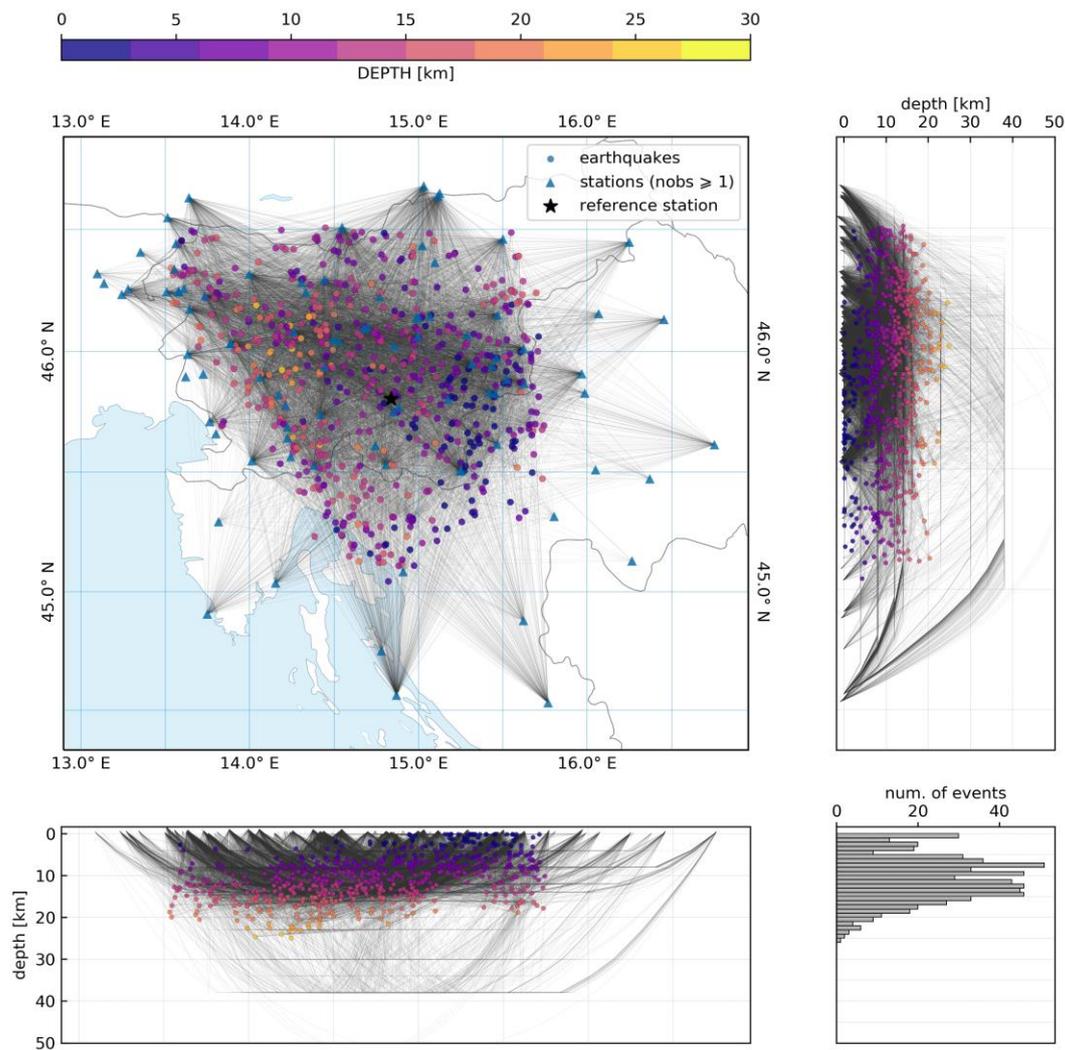
Figure 6: Seismic rays and hypocenters computed for the M2 velocity model. The right and bottom panels show the hypocenters of earthquakes and rays projected on N-S and W-E oriented profiles, respectively. The histogram in the lower right corner shows the number of earthquakes in 1 km depth bins. The seismic stations used in the inversion are also shown.

350
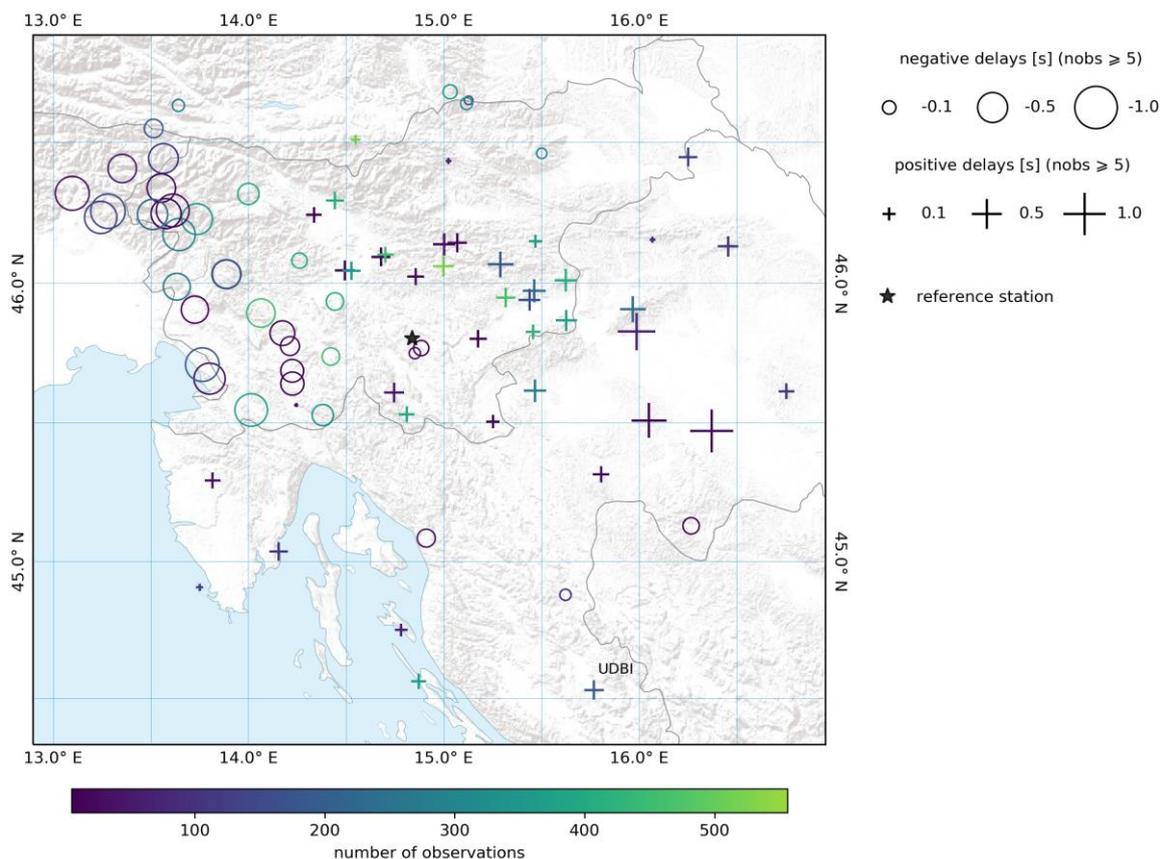
Figure 7: Station delays computed for the M2 velocity model. Station delays are shown only for stations with at least 5 observations. Black star marks the reference station (see main text for details). Shaded relief is shown in the background (Esri, USGS, NOAA).

The two selected models performed better than other models in the stability tests. By varying the velocities of the M2 velocity model by -0.5 km s⁻¹ and performing another inversion run, the average of the differences between the velocities of the model obtained in this test and the final model was -0.03 km s⁻¹ with a standard deviation of 0.03 km s⁻¹ for all layers between 0 and 38 km. For the test with +0.5 km s⁻¹ velocity variation, the average of the velocity differences was 0.03 km s⁻¹ with a standard deviation of 0.04 km s⁻¹. This means that the velocity models obtained in high/low tests converged close to the unshifted model, indicating that stable solutions were obtained for layers between 0 and 38 km depth. Even better convergence after the high/low tests is observed for layers between 4 and 30 km depth (Fig. 8). The hypocenter parameters did not shift by much (Table 1), but as expected there is strong coupling between the station delays and the surface layer velocity.
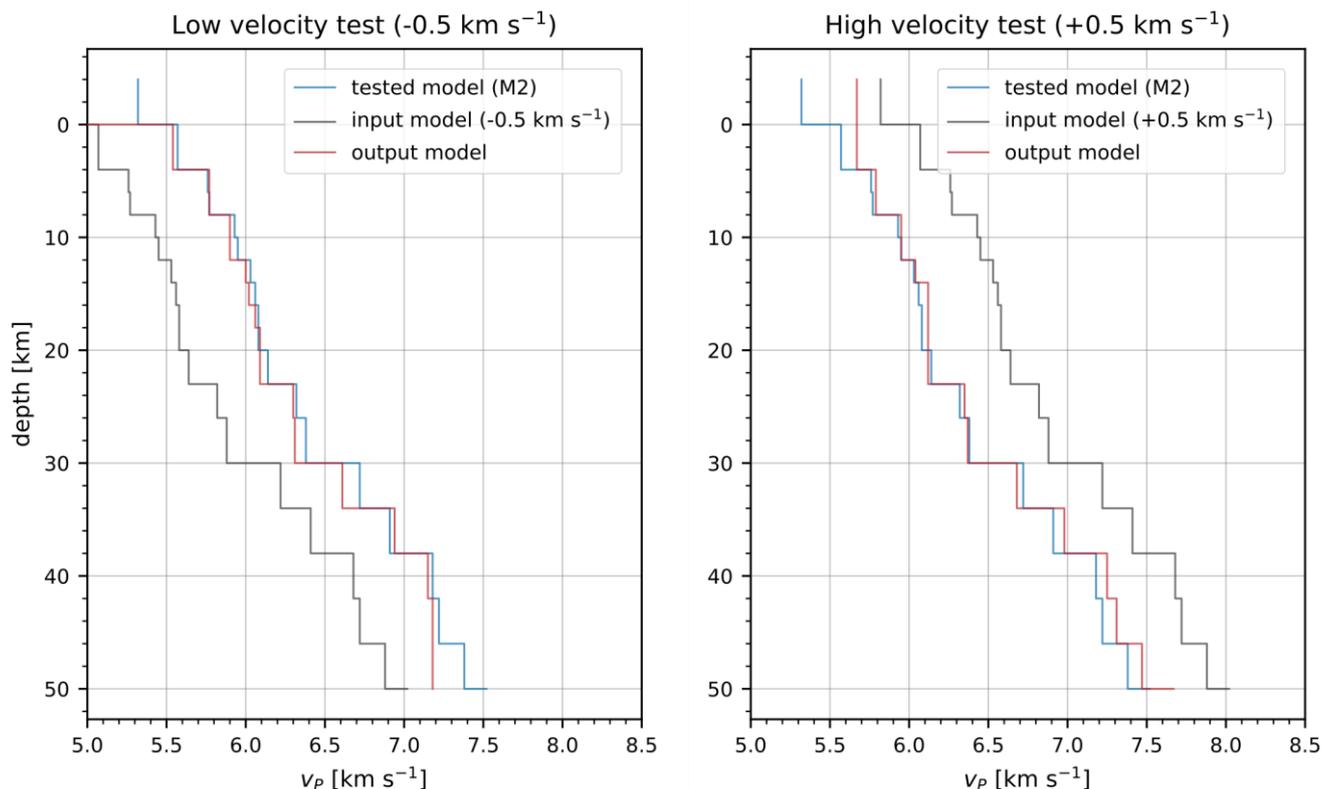
Figure 8: High/low test for the M2 velocity model (blue), where we varied the velocities by ±0.5 km s⁻¹ and used them as the input velocity model (grey) for another inversion run with 9 iterations. The output of this test is shown in red.

370

Table 1: The results of the high/low test for the M2 velocity model, given as average and standard deviation of differences between the values obtained after inversions with the varied models and the final parameter values. The velocity values are calculated only for the well sampled layers between 0 and 38 km. The statistics for the epicenter and hypocenter values were calculated from the lengths of vector differences.

375

Input velocity variation [km s⁻¹]	Epicenter [km]	Hypocenter [km]	Origin time [s]	Velocity [km s⁻¹]	Station delays [s]
-0.5	0.16 ± 0.09	0.48 ± 0.45	-0.04 ± 0.02	-0.03 ± 0.03	0.03 ± 0.03
+0.5	0.15 ± 0.09	0.42 ± 0.36	0.02 ± 0.02	0.03 ± 0.04	0.03 ± 0.02

After performing the systematic and pseudorandom hypocenter shift tests, the hypocenters were mostly relocated close to

380 their initial positions (Fig. 9 and 10), while the velocity model parameters showed very little deviation from their input values (Table 2). Small systematic shifts are observed for the origin times and the velocity parameters, mainly because the earthquake depths were not completely relocated back to their initial positions. This was expected because only P observations were used instead of both P and S observations, making the hypocenter depths less constrained. In addition, the

models that showed less difference in the origin times after the pseudorandom shift test showed a larger deviation in the

385   resulting velocities. The fact that in this test the depth shift was compensated less by a variation in the velocity model and

more in the origin time for the selected models suggests a more stable velocity solution. It also appears that the velocity

parameters are more sensitive to the systematic shift in the input hypocenters. Nevertheless, a small systematic shift of the

hypocenters to shallower depths could also indicate a velocity model that is slightly too fast, or an inability of the method to

converge to the same solution when the hypocenter parameters are shifted by such an amount. Some velocity jumps can also

390   cause rays to refract prematurely, resulting in shorter travel times. For stable solutions we observed very little coupling

between the velocity model and the hypocenter parameters, implying that a variation in the hypocenter parameters or the

velocity model was not compensated by a large variation in the velocity model or the hypocenter parameters, respectively.
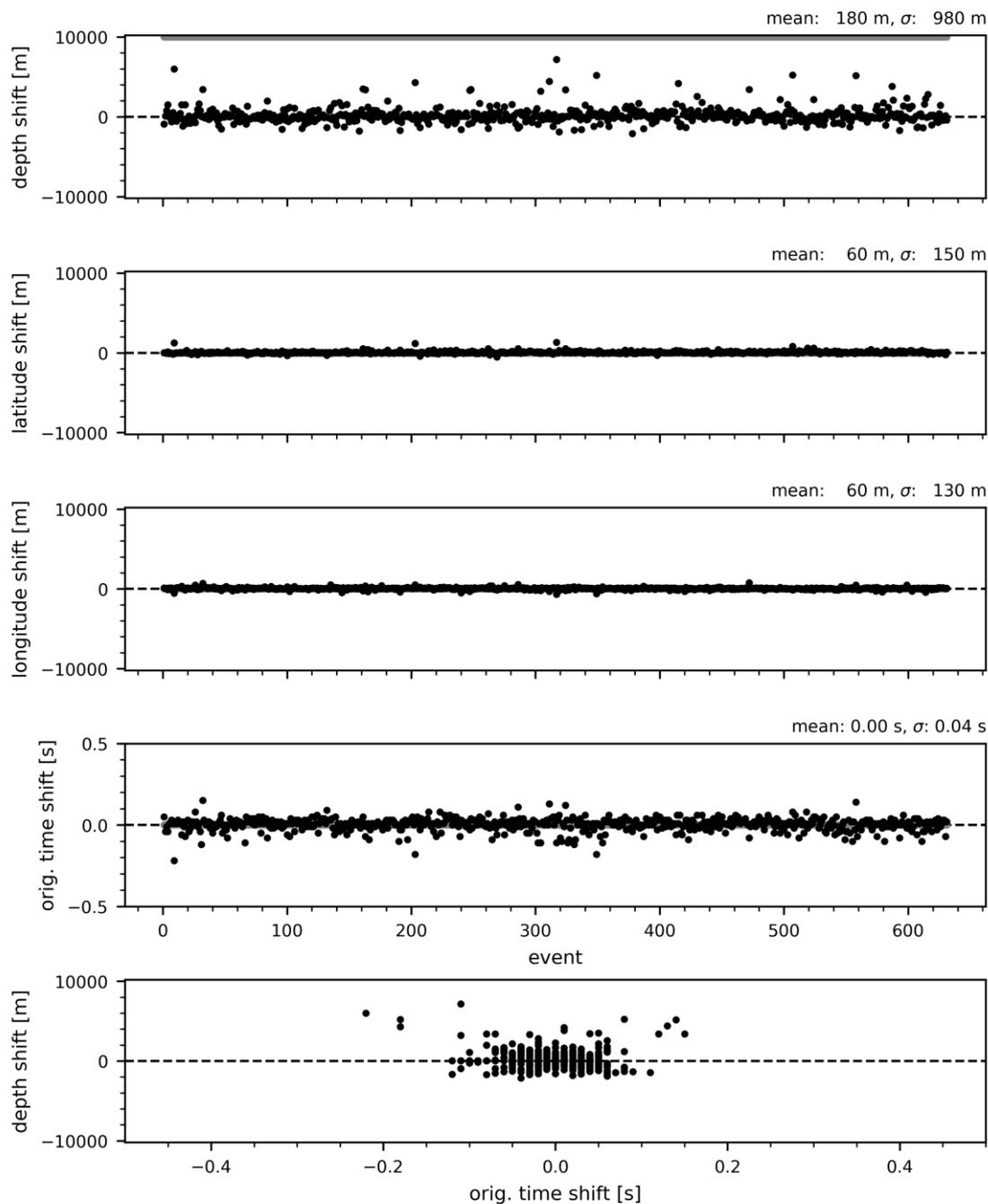
Figure 9: Hypocenter shift test. Hypocenters obtained with the M2 velocity model were shifted systematically in depth by 10 km (grey dots at the top of the first plot) and used as an input in another inversion run with nine iterations. Black dots show the resulting shifts in the hypocenter parameters remaining after this test. All shifts are referenced to hypocenter parameters obtained with the M2 velocity model.
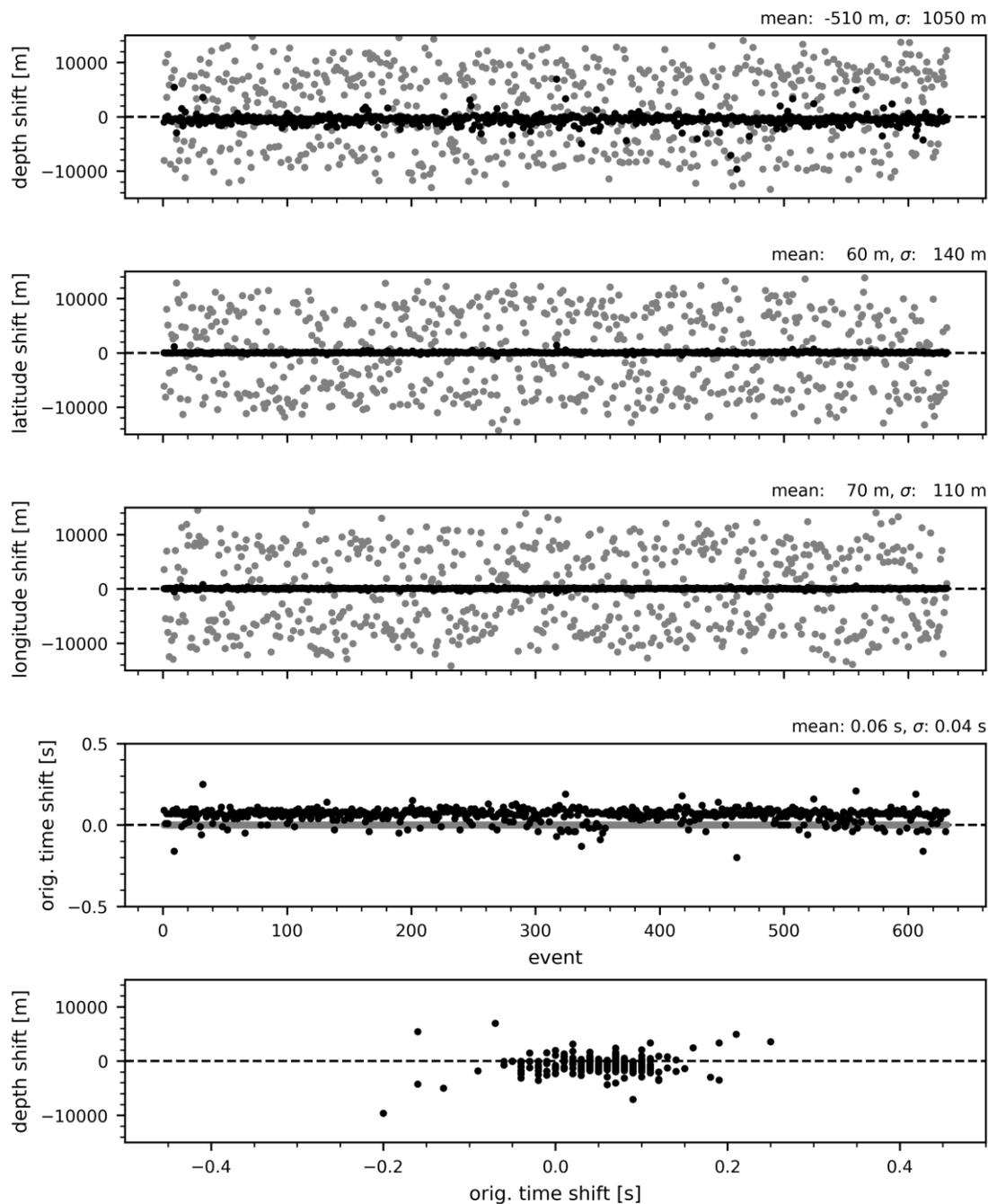
400

Figure 10: Hypocenter shift test. Hypocenters obtained with the M2 velocity model were shifted along pseudorandomly generated vectors by 10 to 15 km (grey dots in the first three plots) and used as an input in another inversion run with nine iterations. Black dots show the resulting shifts in the hypocenter parameters remaining after this test. All shifts are referenced to hypocenter parameters obtained with the M2 velocity model.

405

Table 2: The results of the systematic and pseudorandom hypocenter shift tests for the M2 velocity model, given as average and standard deviation of differences between the values obtained after another inversion and the final parameter values. The velocity values are calculated only for the well sampled layers between 0 and 38 km. The statistics for the epicenter and hypocenter values were calculated from the lengths of vector differences.

Input hypocenter shift [km]	Epicenter [km]	Hypocenter [km]	Origin time [s]	Velocity [km s^{-1}]	Station delays [s]
10 (Z)	0.16 ± 0.14	0.64 ± 0.79	0.00 ± 0.04	-0.05 ± 0.03	0.02 ± 0.02
10-15 (XYZ)	0.15 ± 0.13	0.77 ± 0.90	0.06 ± 0.04	-0.02 ± 0.03	0.02 ± 0.02

410

The RMS residual obtained for the M2 model after the inversion was 0.232 s. We selected 3,215 earthquakes with a maximum azimuthal gap of 180° and at least 10 first P arrival times with uncertainty class less than 3 and relocated them using the velocities and station delays of the M2 model (Fig. 11), obtaining an RMS residual of 0.228 s. Compared to the relocation of the same earthquakes with the routine 1-D velocity model and using the same observations, the reduction in

415 RMS residual is about 20 percent. This reduction is also clearly visible when looking at the residual distribution plot (Fig. S5). A look at the seismicity distribution shows that about 9 percent of the earthquakes were relocated to depths between 0 and 1 km. There are several possible explanations for this. The most obvious is the lack of S arrival times, which would better constrain the depths of the hypocenters. Other reasons include possible overlooked blasts in the data set and unconstrained depths at the periphery of our study area. Most of these earthquakes occurred in southeastern Slovenia,

420 namely in the Krško basin and its surroundings (Fig. S6), which means that the velocity structure in these parts may also bias the depth of hypocenters in these parts. The absence of seismicity at shallow depths in western Slovenia can be observed both in the relocations and in the routinely located seismicity. Conversely, earthquakes in the eastern part of the study area occur at shallower depths and are absent in some parts already below about 10 km.
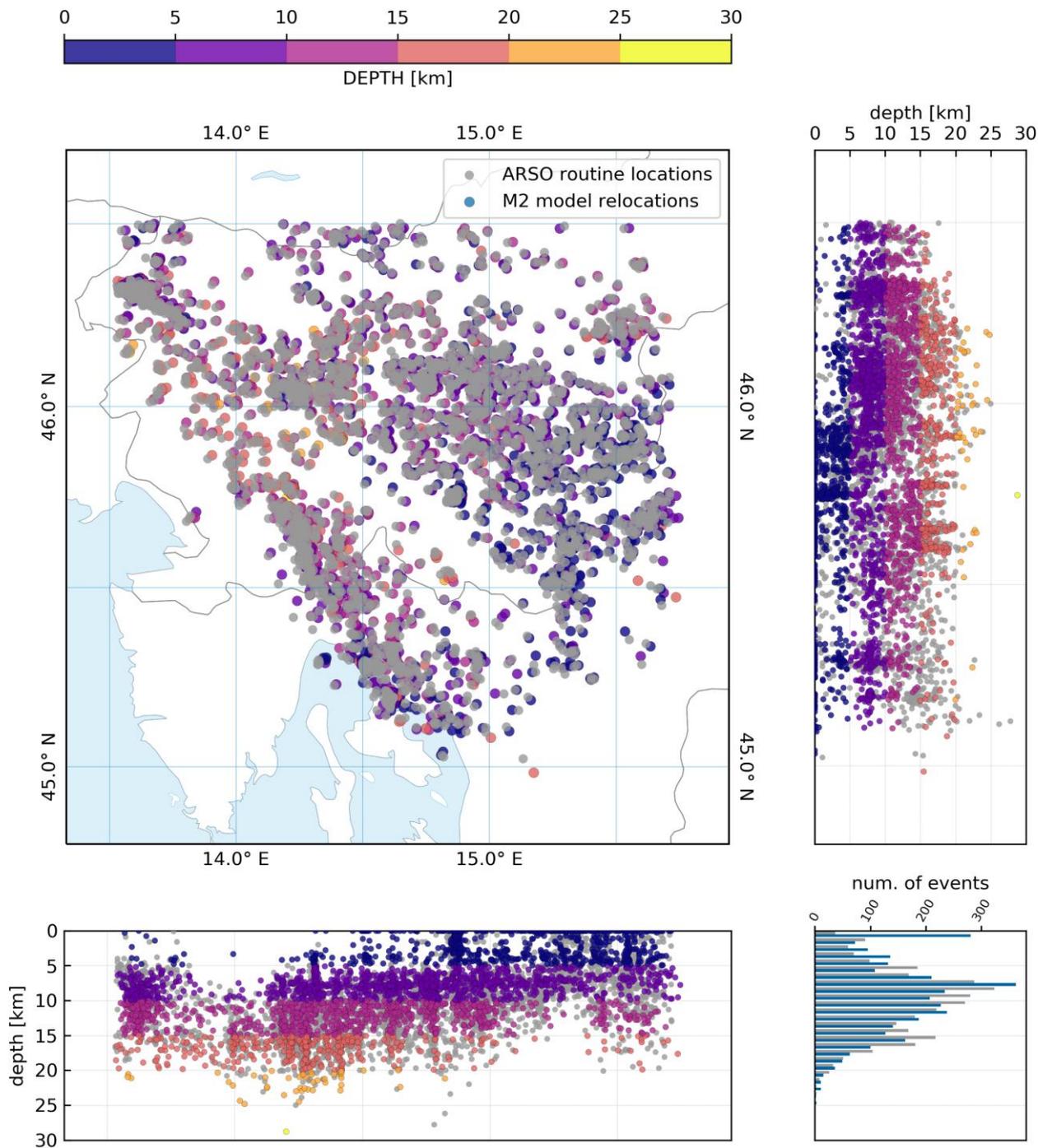
425

Figure 11: Relocation of 3,215 earthquakes with the M2 velocity model (velocities and station delays). The relocation included earthquakes between 2004 and 2018 with a maximum azimuthal gap of 180° and at least 10 first P arrival times with uncertainty

class below 3. The right and bottom panels show the hypocenters of earthquakes projected on N-S and W-E oriented profiles, respectively. The histogram in the lower right corner shows the number of earthquakes in 1 km depth bins for routine locations
430   **(grey) and relocations (blue).**

The relocation of blasts was performed for 107 events with a maximum azimuthal gap of 180° and at least eight first P arrival times with uncertainty class 2 or better (Fig. S7). The average mislocation from known locations is 1.21 and 3.06 km for epicenters and hypocenters, respectively. For all final models, we observe a consistent mislocation of hypocenters to

435   greater depths (below 5 km) for some blasts in southwestern Slovenia.

6.2 Regional subdivision into three subregions

To gain better insight into the crustal velocity structure, we divided the study area into three subregions (Fig. 12), determined mainly on the basis of the station delays (Fig. 7) and the distribution of the relocated seismicity (Fig. 11). We reselected the earthquakes and seismic stations and performed the inversion for each subregion separately. To include more earthquakes in

440   the selection procedure for the southwestern (SW) subregion, we reduced the cell size to 5 km and selected all earthquakes with at least eight first P arrival times. The results of the reselection procedure are shown in Table 3. The inversion procedure was the same as for the regional inversion, but this time we also used the two minimum regional models (M1 and M2) as initial models for the inversion.
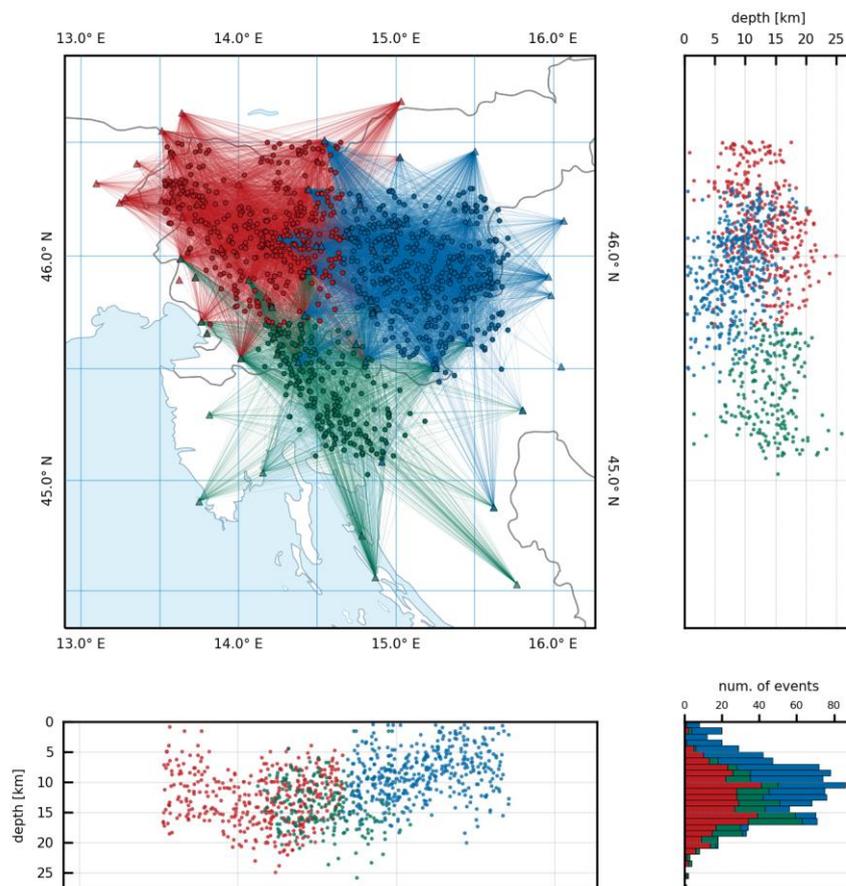
Figure 12: Division of the study area into the eastern (E; blue), northwestern (NW; red), and southwestern (SW; green) subregions. Great-circle rays connecting earthquake station pairs are shown. The right and bottom panels show the hypocenters of earthquakes projected on N-S and W-E oriented profiles, respectively. The histogram in the lower right corner shows the number of earthquakes in 1 km depth bins for each subregion.

450

The velocities of the layers below 23 km are poorly constrained for all subregions (Fig. 13, Tables S8, S9, and S10) because few rays penetrate deeper due to the shorter epicentral distances and because of the relatively shallow seismicity in the region. This resulted in a divergence of the final models below 18 to 23 km for all subregions. Velocity results for the northwestern (NW) subregion show good convergence between 8 and 23 km depth for all models. The layers between 0 and

455   8 km depth show a relatively large difference between the 15th and 85th percentiles, ranging from 0.20 to 0.44 km s⁻¹, compared to the well constrained layers where these values range from 0.06 to 0.15 km s⁻¹. The reason for this is the absence of seismicity in the first 8 km below the surface. Almost the same pattern is observed for the SW subregion. Here, we obtained comparatively better convergence for the layer between 6 and 8 km depth and worse convergence for all other layers between 0 and 23 km, probably due to the smaller number of arrival times and inferior geometry of the seismic

460   stations. While the presence of the shallow earthquakes in the eastern (E) subregion leads to better constrained velocities in

the upper layers, the comparatively smaller number of earthquakes at greater depths leads to divergence occurring already at 18 km depth. For all subregions, we see about 20-34 percent reduction in the RMS residual compared to the regional model. The lowest RMS residual obtained for each subregion is shown in Table 3.

465   **Table 3: Results of the selection procedure and the lowest RMS residuals of the final models obtained for each subregion.**

Region	Number of earthquakes	Number of first P arrivals	Lowest RMS residual for the final models [s]
Northwestern (NW)	393	7,238	0.148
Southwestern (SW)	212	2,396	0.180
Eastern (E)	420	7,466	0.149
Regional	631	15,579	0.225

Median velocities (Fig. 13, Tables S8, S9, and S10) were calculated from the models obtained for a given subregion by excluding the models computed from low and high initial velocity models. Considering the convergence of the obtained models, we focus only on the velocities between 0 and 23 km depth. The median velocities for the E subregion are lower in

470   all resolved layers, especially in the shallow layers. Despite the differences, the median velocities for all subregions are close to the regional median for the layers between 8 and 20 km. Median velocities for the NW and SW subregions are higher and median velocities for the E subregion are lower than the regional median. Besides the velocity jumps between 4 and 8 km depth for the E subregion, we do not observe any other significant velocity jumps in the well-resolved layers for the computed models.

475
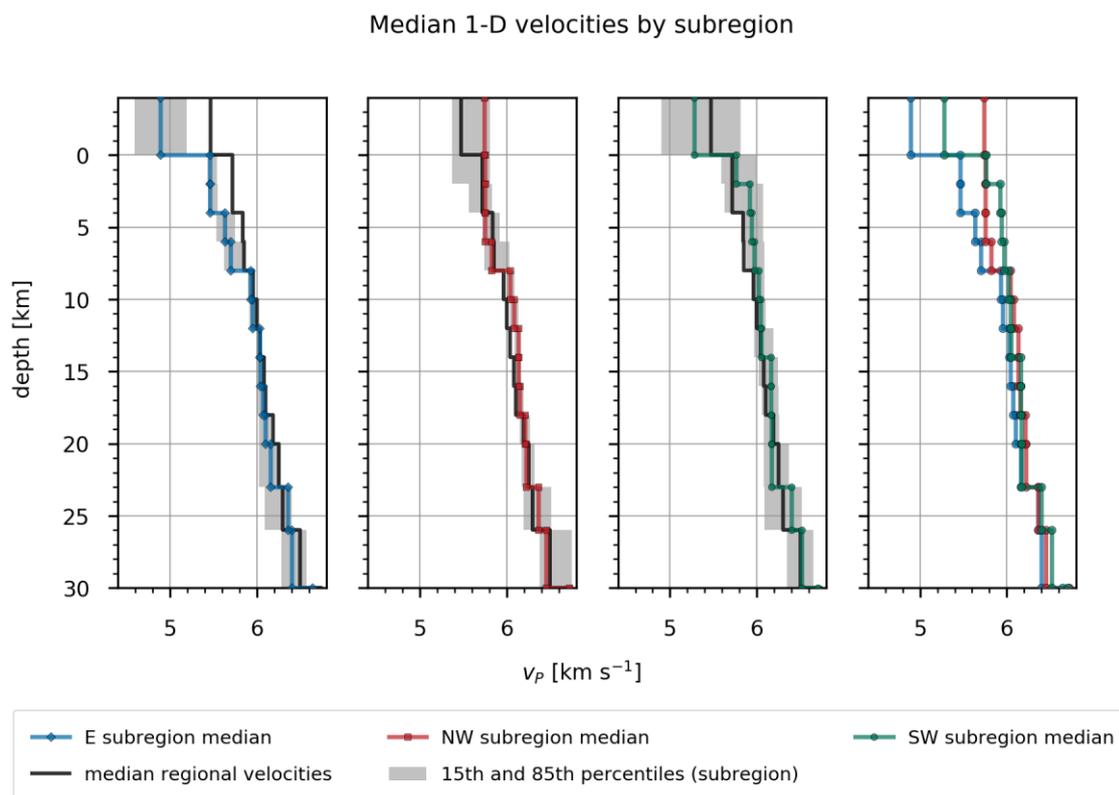
Figure 13: Median velocities calculated from models obtained for a particular subregion. Grey area shows a velocity interval between the 15th and 85th percentiles of all inverted models for each subregion. Corresponding values are given in Tables S8, S9, and S10.

480

7 Discussion and conclusions

One of the goals of this study was to complement the results of previous studies and to expand our knowledge of crustal structure in the region. The seismic ray distribution (Fig. 6) shows that the upper crust is adequately sampled. This was made possible by the modernization of the SNRS (Jesenko & Živčić, 2018) and with the deployment of additional seismic stations

485 in Croatia within the VELEBIT project and the AlpArray project (Molinari et al., 2016). Considering the results of the stability tests and the convergence of the final regional models (Fig. 5) we estimate that a good solution was obtained for depths between 0 and 26 km. The fact that the layers below 26 km were sampled by a comparatively small number of subvertical rays (Fig. 6) limits the ability of the inversion to resolve the velocity structure of the lower crust in more detail.

Nevertheless, the presence of these rays, the convergence of the final models, and the simple velocity structure suggest that
490   at least average velocity has been resolved for depths between 26 and 38 km.

Several features can be observed in the computed regional velocity models. Rather prominent velocity jumps appear at 4 km,
8 km, 23 km, and below 26 km depth (Fig. 5). The largest velocity jumps are observed in the lower crust at interfaces
between 30 and 38 km depth, where the velocity starts to increase more rapidly. As expected, we do not observe a sharp
495   increase in velocity that would indicate a unique depth of the Moho discontinuity. Rather, the depth interval of the rapid
velocity increase indicates a highly variable Moho topography, varying roughly between 30 and 42 km. This is consistent
with previous studies (e.g., Stipčević et al., 2020). The velocity jumps are probably not as pronounced as in reality, as the
velocity in each layer approaches the average of the 3-D velocity variations sampled by the rays. Large lateral variations may
therefore mask large vertical velocity discontinuities, implying that some are likely to have been unresolved by this method.
500   The apparent increase in velocity gradient with depth at 23 to 30 km may indicate the transition from upper to lower crust.

Velocities in the E subregion between 0 and 8 km are much lower compared to the regional median and the median of the
other two subregions (Fig. 13, Tables S8, S9, and S10), indicating the presence of deep sedimentary basins at the periphery
of the Pannonian basin such as the Krško basin. Looking at the individual models for the E subregion, we consistently
505   observe a slow increase in velocity between 8 and 12 km depth and almost no increase in velocity between 12 and 23 km
depth, similar to what Živčić et al. (2000) observed for eastern Slovenia. Compared to the other two subregions, velocities in
the E subregion are lower throughout the upper 20 km of the crust. This agrees well with the previous studies (Michelini et
al., 1998; Živčić et al., 2000; Brückl et al., 2007; Brückl et al., 2010; Kapuralić et al., 2019) and could be caused by
increased heat flow due to the thinner crust or by the presence of a low velocity body in the upper crust. The first explanation
510   would be consistent with the extensional event (Ratschbacher, 1991a, 1991b; Horváth & Cloetingh, 1996) that led to the
formation of the Pannonian basin and also affected some adjacent units. Despite poorly constrained velocities between 2 and
8 km depth, individual models consistently show lower velocities for the NW subregion than for the SW subregion. At least
to some extent, we could explain these differences by the presence of sedimentary basins in central and northwestern
Slovenia (NW subregion) or thicker carbonate rock cover in the SW subregion. The NW and SW subregions are very similar
515   in terms of crustal structure between about 8 and 23 km depth and differ only slightly in the rate of velocity increase between
14 or 16 and 23 km depth. Depth intervals with slow velocity increase, ranging from 6 to 15 km, are observed between about
8 and 23 km depth in all subregional models. Such features could result from thick homogeneous layers where seismic
velocity is mainly controlled by pressure and temperature gradient.

520   In terms of absolute seismic velocities, the obtained velocity models show much higher velocities above 30 km compared to
the R1D model (Fig. 14). The only models with lower velocities compared to the routine model are those obtained for the E
subregion, and even in this case only above 6 km depth. The results for the subregions can be compared with some velocity

models obtained in previous studies. As already observed by Michelini et al. (1998), we see that velocities in the upper 6 km differ significantly between western and eastern Slovenia. We also obtained similar absolute velocity values in the first 6 km

525   of the crust. The velocities of the deeper crust in the west, at 13 and 20 km, obtained by Michelini et al. (1998) also agree well with our results, but on the other hand we obtained higher velocities for the E subregion. The velocities in the deeper parts of the E subregion seem to be more in agreement with the velocity values obtained by Kapuralić et al. (2019). Velocities in regional models at depths between 23 and 30 km are consistent with the transition from upper to lower crust as defined by Magrin & Rossi (2020) for the northern Adria, including the NW Dinarides. The transition was interpreted to

530   occur at a P wave velocity of about 6.4 km s^{-1}. The velocities in their 3-D model at the point near the reference station for our regional inversion (NAC2 14.86E 45.83N) agree very well with the velocities of our median regional velocities throughout the crust. Good agreement with the results of Magrin & Rossi (2020; NAC2 14.28E 46.05N) is also observed between 8 and 30 km depth for the median velocities of the NW subregion. In this depth interval the median velocities of the NW subregion are also very close to the velocities obtained by Brückl et al. (2007; ALP01 460 and 520 km). The model of Magrin & Rossi

535   (2020, NAC2 14.35E 45.51N) also closely resembles the median velocities of the SW subregion. The largest differences are above 6 km and between 18 and 23 km depth. Velocities extracted at 300 km along the ALP02 profile of Brückl et al. (2007) fit well with our median velocities for the E subregion below 6 km. The discrepancy above 6 km appears due to the large lateral variations in these layers, while the velocities in the published model were extracted at one point. The same is true for the other two subregions. The model of Šumanovac (2010), on the other hand, shows large discrepancies with our results.

540

The pattern of computed station delays (Fig. 7) agrees very well with the map of sediment delay times compiled by Behm et al. (2009). The only station delays that do not match the sediment delay times belong to the seismic stations on the Istra peninsula. These positive station delays could be related to the relatively low velocities at shallow depths seen in the velocity models of Guidarelli et al. (2017) and Kapuralić et al. (2019), or to large-scale variations in the crust due to the limited

545   azimuthal coverage of the observations. The travel times calculated for the southernmost two stations correspond mostly to the rays refracted at 40 km depth and above (Fig. 6). According to Stipčević et al. (2020), the Moho is deeper in this region, which means that the observed travel times are larger than calculated due to longer refracted ray paths, leading to positive station delays. Some shallower refractions at these stations are also likely the result of velocity jumps in the lower crust that occur in the regional models due to the shallowing of the Moho towards the Pannonian basin. These velocity jumps are

550   probably not present in the area of the southernmost stations and therefore contribute to the occurrence of the positive station delays. Based on the results for the subregions, the study area cannot be considered uniform from the seismic velocity and seismicity point of view. This means that using only one model to locate earthquakes at the regional scale may bias the hypocenters, even with the computed station delays. As can be seen from our study, the station delays cannot always account for the full effect that lateral velocity variations in the shallow crust have on travel times, especially in the case of deep

555   sedimentary basins.
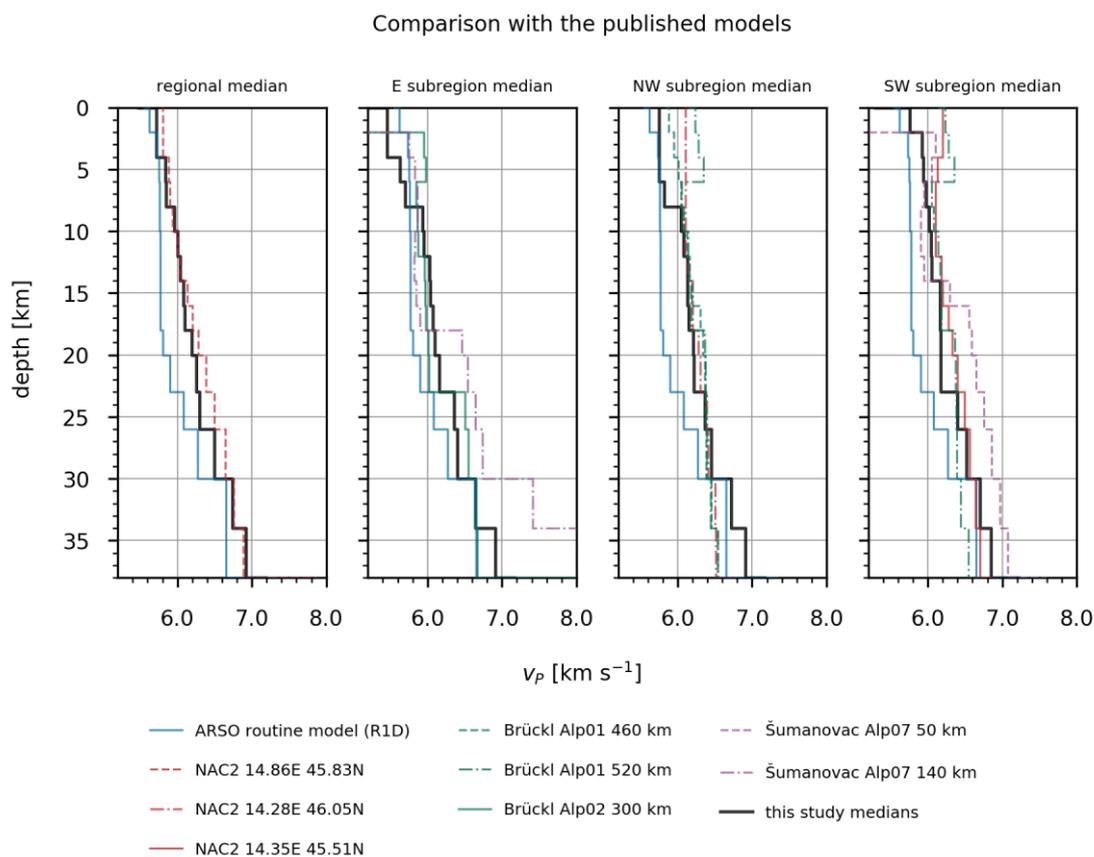
Figure 14: Comparison of the median velocity models obtained in this study (black lines) with the published models from Brückl et al. (2007), Magrin & Rossi (2020), Šumanovac (2010) and the routine model. Models based on the results of Magrin & Rossi (2020; NAC2) were extracted at the point closest to the respective reference seismic station. Kilometres denote the distance along the profiles in Brückl et al. (2007) and Šumanovac (2010). For easier comparison, all published models were extracted by calculating the weighted average of the velocities in each layer.

In the western part of the study area, the seismicity relocated with the M2 model (Fig. 11) is constrained to depths between 5 and 20 km, which corresponds to the depths determined by Vičič et al. (2019) for western Slovenia. Towards the eastern part of the study area, the earthquake hypocenters become shallower, in agreement with the Moho depth, as already suggested by Stipčević et al. (2020). Moreover, it appears that most of the seismicity in the region is constrained to the depths between the main velocity jumps in the upper crust. Therefore, the velocity jumps at the transition to the lower crust suggest a change in physical properties that inhibits the occurrence of deeper earthquakes. A similar observation has already been made by Magrin & Rossi (2020), who tied the spatial seismicity distribution in the northern part of Adria to the changes in different physical parameters in the crust. A look at the depth distribution of the relocated seismicity shows that about 9 percent of the earthquakes were relocated to depths between 0 and 1 km. Most of these earthquakes occurred in southeastern Slovenia,

namely in the Krško basin and its surroundings (Fig. S6). Relocating these earthquakes with one of the velocity models (velocities and station delays) computed for the E subregion largely mitigated this problem. This shows that the shallow
575   structure was more accurately resolved with the inversion on a smaller scale, as also previously shown by Husen et al. (2011). Lower RMS residuals obtained for the subregions also indicate a better fit of the obtained velocities and better resolved station delays, as there are relatively fewer differences between the structure below the reference station and other stations. The division into subregions allows us to further investigate ray sampling and seismicity distribution of each subregion, which in turn allows better preparation for 3-D tomography. The gap in seismicity between 5 and 10 km depth in
580   the western part of our study area can be observed in both the relocated and routinely located seismicity. In the east, there is a gap in seismicity deeper in the crust between about 10 and 15 km depth. Since earthquakes occurred in the other parts of the study area at comparable depths, the apparent absence of earthquakes could be due to the relatively short time span of our data set. If there are any structural reasons for this type of depth distribution, we expect to find them with the computation of a 3-D velocity model.

585

With this study, we evaluated in detail the performance of 1-D inversion, which has been shown many times to be essential for the results of LET (e.g., Kissling et al., 1994). The obtained 1-D regional and several local velocity models provide reliable and fast hypocenter locations of local events using only P arrival times. Further work is needed in the study area to obtain an independent 1-D S velocity model and to continue the study of the Dinarides further south, where the data
590   selection process will be more challenging due to the smaller number of seismic stations. Based on the evidence of the highly variable Vp/Vs ratio in the study area (Stipčević et al., 2020), independent P and S velocity models could provide an improvement for the relocation of the seismicity compared to the constant ratio often used in studies of this region. This could be partially confirmed by multiplying the S wave velocities of Živčić et al. (2000) by a constant Vp/Vs ratio value of 1.73 and comparing these P velocity proxies with the velocity values estimated here for the respective subregions. Doing so,
595   we observe the largest discrepancy above 12 km and very good agreement below 12 km. This discrepancy of the Vp/Vs ratio in the shallower layers could be caused by the saturated sedimentary layers. The results of this study will also be used to compute a high-resolution 3-D velocity model that has the potential to resolve tectonic structures in the upper crust in more detail and to link tectonics to seismicity.

600   *Code and data availability.* Routine hypocenter locations were obtained using the HYPOCENTER program (Lienert & Havskov, 1995). Hypocenter-velocity inversions were performed using the shareware program VELEST (Kissling et al., 1994). Figures and maps were plotted in Python using Matplotlib and Cartopy packages.

Seismic bulletins and catalogues: Earthquake information is provided by the Slovenian Environment Agency
605   (ARSO, seismological bulletin 2004-2018 and earthquake information), University of Zagreb (earthquake information), and

GEOFON data centre of the GFZ German Research Centre (https://geofon.gfz-potsdam.de/, last access: May 2021; earthquake information).

Permanent seismic networks:

610   INGV Seismological Data Centre: Rete Sismica Nazionale (RSN), Istituto Nazionale di Geofisica e Vulcanologia (INGV), Italy, https://doi.org/10.13127/SD/X0FXnH7QfY, 2006.

MedNet Project Partner Institutions: Mediterranean Very Broadband Seismographic Network (MedNet), Istituto Nazionale di Geofisica e Vulcanologia (INGV), https://doi.org/10.13127/SD/fBBBtDtd6q, 1990.

OGS (Istituto Nazionale Di Oceanografia E Di Geofisica Sperimentale) And University of Trieste: North-East Italy
615   Broadband Network, International Federation of Digital Seismograph Networks, https://doi.org/10.7914/SN/NI, 2002.

OGS (Istituto Nazionale Di Oceanografia E Di Geofisica Sperimentale): North-East Italy Seismic Network, International Federation of Digital Seismograph Networks, https://doi.org/10.7914/SN/OX, 2016.

Slovenian Environment Agency: Seismic Network of the Republic of Slovenia, International Federation of Digital Seismograph Networks, https://doi.org/10.7914/SN/SL, 2001.

620   University of Zagreb: Croatian Seismograph Network, International Federation of Digital Seismograph Networks, https://doi.org/10.7914/SN/CR, 2001.

ZAMG-Zentralanstalt Für Meteorologie Und Geodynamik: Austrian Seismic Network, International Federation of Digital Seismograph Networks, https://doi.org/10.7914/SN/OE, 1987.

625   *Temporary seismic networks:*
AlpArray Seismic Network: AlpArray Seismic Network (AASN) temporary component, AlpArray Working, https://doi.org/10.12686/alparray/z3_2015, 2015.

Team list

The complete member list of the AlpArray Working Group:

630   György Hetényi, Rafael Abreu, Ivo Allegretti, Maria-Theresia Apoloner, Coralie Aubert, Simon Besançon, Maxime Bès De Berc, Götz Bokelmann, Didier Brunel, Marco Capello, Martina Čarman, Adriano Cavaliere, Jérôme Chèze, Claudio Chiarabba, John Clinton, Glenn Cougoulat, Wayne C. Crawford, Luigia Cristiano, Tibor Czifra, Ezio D'alema, Stefania Danesi, Romuald Daniel, Anke Dannowski, Iva Dasović, Anne Deschamps, Jean-Xavier Dessa, Cécile Doubre, Sven

Egdorf, Ethz-Sed Electronics Lab, Tomislav Fiket, Kasper Fischer, Wolfgang Friederich, Florian Fuchs, Sigward Funke, Domenico Giardini, Aladino Govoni, Zoltán Gráczer, Gidera Gröschl, Stefan Heimers, Ben Heit, Davorka Herak, Marijan Herak, Johann Huber, Dejan Jarić, Petr Jedlička, Yan Jia, Hélène Jund, Edi Kissling, Stefan Klingen, Bernhard Klotz, Petr Kolínský, Heidrun Kopp, Michael Korn, Josef Kotek, Lothar Kühne, Krešo Kuk, Dietrich Lange, Jürgen Loos, Sara Lovati, Deny Malengros, Lucia Margheriti, Christophe Maron, Xavier Martin, Marco Massa, Francesco Mazzarini, Thomas Meier, Laurent Métral, Irene Molinari, Milena Moretti, Anna Nardi, Jurij Pahor, Anne Paul, Catherine Péquegnat, Daniel Petersen, Damiano Pesaresi, Davide Piccinini, Claudia Piromallo, Thomas Plenefisch, Jaroslava Plomerová, Silvia Pondrelli, Snježan Prevolnik, Roman Racine, Marc Régnier, Miriam Reiss, Joachim Ritter, Georg Rümpker, Simone Salimbeni, Marco Santulin, Werner Scherer, Sven Schippkus, Detlef Schulte-Kortnack, Vesna Šipka, Stefano Solarino, Daniele Spallarossa, Kathrin Spieker, Josip Stipčević, Angelo Strollo, Bálint Süle, Gyöngyvér Szanyi, Eszter Szűcs, Christine Thomas, Martin Thorwart, Frederik Tilmann, Stefan Ueding, Massimiliano Vallocchia, Luděk Vecsey, René Voigt, Joachim Wassermann, Zoltán Wéber, Christian Weidle, Viktor Wesztergom, Gauthier Weyland, Stefan Wiemer, Felix Wolf, David Wolyniec, Thomas Zieke, Mladen Živčić, Helena Žlebčíková.

Author contributions. G.R., J.S., M.Ž., and A.G. conceptualised the study. G.R. performed the inversion, programmed supporting algorithms, developed the tests, prepared the figures, and wrote the original draft of the manuscript. G.R., J.S., M.Ž., and M.H. validated the results. G.R., J.S., M.Ž., M.H., and A.G. curated the data and were involved in investigation. A.G. supervised the study and acquired funding. All co-authors discussed the methods and results and reviewed and edited the manuscript. The AlpArray Working Group provided access to seismic data from the temporary stations.

Competing interests. The authors declare that they have no conflict of interest.

Acknowledgments. This study was conducted with the support of the Research Program P1-0011 and Young Researcher grant (1000-21-0510) financed by the Slovenian Research Agency. Many thanks to Edi Kissling and Matteo Bagagli for providing the latest version of VELEST code and for discussion. We also thank Emanuel Kästle for providing base geology and tectonics layers.

References

Aki, K., Christoffersson, A., and Husebye, E. S.: Determination of 3-dimensional seismic structure of lithosphere, Journal of Geophysical Research, 82, 277-296, https://doi.org/10.1029/JB082i002p00277, 1977.

Behm, M.: 3-D modelling of the crustal S-wave velocity structure from active source data: application to the Eastern Alps and the Bohemian Massif, Geophysical Journal International, 179, 265-278, https://doi.org/10.1111/j.1365-246X.2009.04259.x, 2009.

Behm, M., Bruckl, E., Chwatal, W., and Thybo, H.: Application of stacking and inversion techniques to three-dimensional wide-angle reflection and refraction seismic data of the Eastern Alps, Geophysical Journal International, 170, 275-298, https://doi.org/10.1111/j.1365-246X.2007.03393.x, 2007.

Belinić, T., Stipčević, J., Živčić, M., and AlpArrayWorking, G.: Lithospheric thickness under the Dinarides, Earth and Planetary Science Letters, 484, 229-240, https://doi.org/10.1016/j.epsl.2017.12.030, 2018.

Brückl, E., Bleibinhaus, F., Gosar, A., Grad, M., Guterch, A., Hrubcova, P., Keller, G. R., Majdanski, M., Šumanovac, F., Tiira, T., Yliniemi, J., Hegedus, E., and Thybo, H.: Crustal structure due to collisional and escape tectonics in the Eastern Alps region based on profiles Alp01 and Alp02 from the ALP 2002 seismic experiment, Journal of Geophysical Research-Solid Earth, 112, https://doi.org/10.1029/2006JB004687, 2007.

Brückl, E., Behm, M., Decker, K., Grad, M., Guterch, A., Keller, G. R., and Thybo, H.: Crustal structure and active tectonics in the Eastern Alps, Tectonics, 29, https://doi.org/10.1029/2009TC002491, 2010.

Cecić, I. and Jocif, J.: Idrijski potres 26. marca 1511. Geografski obzornik, 58(1), 24-29, 2011.

Cecić, I., Nečak, D., and Berus, M.: Ob 101. obletnici brežiškega potresa, Ujma, 32, 200-209, 2018.

Crosson, R. S.: Crustal structure modeling of earthquake data: 1. Simultaneous least squares estimation of hypocenter and velocity parameters, Journal of Geophysical Research, 81, 3036-3046, https://doi.org/10.1029/JB081i017p03036, 1976.

Diehl, T., Husen, S., Kissling, E., and Deichmann, N.: High-resolution 3-D P-wave model of the Alpine crust, Geophysical Journal International, 179, 1133-1147, https://doi.org/10.1111/j.1365-246X.2009.04331.x, 2009.

Fitzko, F., Suhadolc, P., Aoudia, A., and Panza, G. F.: Constraints on the location and mechanism of the 1511 Western-Slovenia earthquake from active tectonics and modeling of macroseismic data, Tectonophysics, 404, 77-90, https://doi.org/10.1016/j.tecto.2005.05.003, 2005.

Fodor, L., Csontos, L., Bada, G., Györfi, I., and Benkovics, L.: Tertiary tectonic evolution of the Pannonian Basin system and neighbouring orogens: a new synthesis of palaeostress data, Geological Society, London, Special Publications, 156, 295, https://doi.org/10.1144/GSL.SP.1999.156.01.15, 1999.

Guidarelli, M., Aoudia, A., and Costa, G.: 3-D structure of the crust and uppermost mantle at the junction between the
690   Southeastern Alps and External Dinarides from ambient noise tomography, Geophysical Journal International, 211, 1509-
1523, https://doi.org/10.1093/gji/ggx379, 2017.

Handy, M. R., Schmid, S. M., Bousquet, R., Kissling, E., and Bernoulli, D.: Reconciling plate-tectonic reconstructions of
Alpine Tethys with the geological-geophysical record of spreading and subduction in the Alps, Earth-Science Reviews, 102,
121-158, https://doi.org/10.1016/j.earscirev.2010.06.002, 2010.

695   Handy, M. R., Ustaszewski, K., and Kissling, E.: Reconstructing the Alps-Carpathians-Dinarides as a key to understanding
switches in subduction polarity, slab gaps and surface motion, International Journal of Earth Sciences, 104, 1-26,
https://doi.org/10.1007/s00531-014-1060-3, 2015.

Haslinger, F., Kissling, E., Ansorge, J., Hatzfeld, D., Papadimitriou, E., Karakostas, V., Makropoulos, K., Kahle, H. G., and
Peter, Y.: 3D crustal structure from local earthquake tomography around the Gulf of Arta (Ionian region, NW Greece),
700   Tectonophysics, 304, 201-218, https://doi.org/10.1016/S0040-1951(98)00298-4, 1999.

Herak, M., Herak, D., and Markušić, S.: Revision of the earthquake catalogue and seismicity of Croatia, 1908-1992, Terra
Nova, 8, 86-94, https://doi.org/10.1111/j.1365-3121.1996.tb00728.x, 1996.

Herak, D., Sović, I., Cecić, I., Živčić, M., Dasović, I., and Herak, M.: Historical Seismicity of the Rijeka Region (Northwest
External Dinarides, Croatia) - Part I: Earthquakes of 1750, 1838, and 1904 in the Bakar Epicentral Area, Seismological
705   Research Letters, 88, 904-915, https://doi.org/10.1785/0220170014, 2017.

Herak, M., Živčić, M., Sović, I., Cecić, I., Dasović, I., Stipčević, J., and Herak, D.: Historical Seismicity of the Rijeka
Region (Northwest External Dinarides, Croatia) - Part II: The Klana Earthquakes of 1870, Seismological Research Letters,
89, 1524-1536, https://doi.org/10.1785/0220180064, 2018.

Horvath, F. and Cloetingh, S.: Stress-induced late-stage subsidence anomalies in the Pannonian basin, Tectonophysics, 266,
710   287-300, https://doi.org/10.1016/S0040-1951(96)00194-1, 1996.

Husen, S., Kissling, E., Flueh, E., and Asch, G.: Accurate hypocentre determination in the seismogenic zone of the
subducting Nazca Plate in northern Chile using a combined on-/offshore network, Geophysical Journal International, 138,
687-701, https://doi.org/10.1046/j.1365-246x.1999.00893.x, 1999.

Husen, S., Kissling, E., and Clinton, J. F.: Local and regional minimum 1D models for earthquake location and data quality
715 assessment in complex tectonic regions: application to Switzerland, Swiss Journal of Geosciences, 104, 455-469,
https://doi.org/10.1007/s00015-011-0071-3, 2011.

Ivančić, I., Herak, D., Herak, M., Allegretti, I., Fiket, T., Kuk, K., Markušić, S., Prevolnik, S., Sović, I., Dasović, I., and
Stipčević, J.: Seismicity of Croatia in the period 2006-2015, Geofizika, 35, 69-98,
https://doi.org/10.15233/gfz.2018.35.2, 2018.

720 Jesenko, T. and Živčić, M.: Nekateri rezultati prenove državne mreže potresnih opazovalnic, in: Potresi v letu
2016/Earthquakes in 2016, edited by: Gosar, A., Slovenian Environment Agency (ARSO), Ljubljana, Slovenia, 53-68, 2018,

Kapuralić, J., Šumanovac, F., and Markušić, S.: Crustal structure of the northern Dinarides and southwestern part of the
Pannonian basin inferred from local earthquake tomography, Swiss Journal of Geosciences, 112, 181-198,
https://doi.org/10.1007/s00015-018-0335-2, 2019.

725 Kissling, E.: Geotomography with local earthquake data, Reviews of Geophysics, 26, 659-698,
https://doi.org/10.1029/RG026i004p00659, 1988.

Kissling, E., Ellsworth, W. L., Eberhart-Phillips, D., and Kradolfer, U.: Initial reference models in local earthquake
tomography, Journal of Geophysical Research-Solid Earth, 99, 19635-19646, https://doi.org/10.1029/93JB03138, 1994.

Kissling, E., Kradolfer, U., and Maurer, H.: VELEST User's Guide – Short Introduction, Institute of geophysics and Swiss
730 seismological service, User Guide, ETH, Zürich, 1995.

Kissling, E., Schmid, S. M., Lippitsch, R., Ansorge, J., and Fügenschuh, B.: Lithosphere structure and tectonic evolution of
the Alpine arc: new evidence from high-resolution teleseismic tomography, Geological Society, London, Memoirs, 32, 129,
https://doi.org/10.1144/GSL.MEM.2006.032.01.08, 2006.

Korbar, T.: Orogenic evolution of the External Dinarides in the NE Adriatic region: a model constrained by
735 tectonostratigraphy of Upper Cretaceous to Paleogene carbonates, Earth-Science Reviews, 96, 296-312.
https://doi.org/10.1016/j.earscirev.2009.07.004, 2009.

Lapajne, J.: Veliki potresi na Slovenskem – II, Ujma, 2, 70-74, 1988.

Lapajne, J.: Veliki potresi na Slovenskem – III, Ujma, 3, 55-61, 1989.

Lienert, B. R. and Havskov, J.: A Computer Program for Locating Earthquakes Both Locally and Globally. Seismological
740 Research Letters, 66(5), 26–36. https://doi.org/10.1785/gssrl.66.5.26, 1995.

Magrin, A. and Rossi, G.: Deriving a New Crustal Model of Northern Adria: The Northern Adria Crust (NAC) Model.
Frontiers in Earth Science, 8(89), https://doi.org/10.3389/feart.2020.00089, 2020.

Markušić, S.: Seismicity of Croatia, in: Earthquake Monitoring and Seismic Hazard Mitigation in Balkan Countries :
Proceedings of the NATO Advanced Research Workshop on Earthquake Monitoring and Seismic Hazard Mitigation in
745 Balkan Countries, edited by: Husebye, E. S., Springer, NATO Science Series, IV: Earth and Environmental Sciences,
Dordrecht, Netherlands, 81, 81-98, https://doi.org/10.1007/978-1-4020-6815-7_5, 2008.

Márton, E.: Paleomagnetic evidence for Tertiary counterclockwise rotation of adria with respect to africa, in: The Adria
Microplate: GPS Geodesy, Tectonics and Hazards, edited by: Pinter, N., Gyula, G., Weber, J., Stein, S., and Medak, D.,
NATO Science Series, IV: Earth and Environmental Sciences, Dordrecht, Netherlands, 61, 71-80,
750 https://doi.org/10.1007/1-4020-4235-3_05, 2006.

Márton, E., Drobne, K., Ćosović, V., and Moro, A.: Palaeomagnetic evidence for Tertiary counterclockwise rotation of
Adria, Tectonophysics, 377, 143-156, https://doi.org/10.1016/j.tecto.2003.08.022, 2003.

Maurer, V., Kissling, E., Husen, S., and Quintero, R.: Detection of Systematic Errors in Travel-Time Data Using a Minimum
1D Model: Application to Costa Rica Seismic Tomography, Bulletin of the Seismological Society of America, 100, 629-639,
755 https://doi.org/10.1785/0120090032, 2010.

Michelini, A., Živčić, M., and Suhadolc, P.: Simultaneous inversion for velocity structure and hypocenters in Slovenia,
Journal of Seismology, 2, 257-265. https://doi.org/10.1023/A:1009723017040, 1998.

Molinari, I., Clinton, J., Kissling, E., Hetényi, G., Giardini, D., Stipčević, J., Dasović, I., Herak, M., Šipka, V., Wéber, Z.,
Gráczer, Z., Solarino, S., the Swiss-AlpArray Field Team, and the AlpArray Working Group.: Swiss-AlpArray temporary
760 broadband seismic stations deployment and noise characterization, Advances in Geosciences, 43, 15–29,
https://doi.org/10.5194/adgeo-43-15-2016, 2016.

Pamić, J., Gušić, I., and Jelaska, V.: Geodynamic evolution of the central Dinarides, Tectonophysics, 297, 251-268,
https://doi.org/10.1016/S0040-1951(98)00171-1, 1998.

Pavlis, G. L. and Booker, J. R.: A study of the importance of nonlinearity in the inversion of earthquake arrival time data for
765 velocity structure, Journal of Geophysical Research, 88, 5047-5055, https://doi.org/10.1029/JB088iB06p05047, 1983.

Picha, F. J.: Late orogenic strike-slip faulting and escape tectonics in frontal Dinafides-Hellenides, Croatia, Yugoslavia, Albania, and Greece, Aapg Bulletin, 86, 1659-1671, https://doi.org/10.1306/61EEDD32-173E-11D7-8645000102C1865D, 2002.

Placer, L., Vrabec, M., and Celarc, B.: The bases for understanding of the NW Dinarides and Istria Peninsula tectonics.
770 Geologija, 53/1, 55-86, 2010.

Poljak, M., Zivčić, M., and Zupančič, P.: The seismotectonic characteristics of Slovenia, Pure and Applied Geophysics, 157, 37-55, https://doi.org/10.1007/PL00001099, 2000.

Ratschbacher, L., Merle, O., Davy, P., and Cobbold, P.: Lateral extrusion in the eastern Alps, Part 1: Boundary conditions and experiments scaled for gravity, Tectonics, 10, 245-256, https://doi.org/10.1029/90TC02622, 1991a.

775 Ratschbacher, L., Frisch, W., Linzer, H. G., and Merle, O.: Lateral extrusion in the eastern Alps, Part 2: Structural analysis, Tectonics, 10, 257-271, https://doi.org/10.1029/90TC02623, 1991b.

Schmid, S. M., Fügenschuh, B., Kissling, E., and Schuster, R.: Tectonic map and overall architecture of the Alpine orogen, Eclogae Geologicae Helvetiae, 97, 93-117, https://doi.org/10.1007/s00015-004-1113-x, 2004.

Schmid, S. M., Bernoulli, D., Fügenschuh, B., Matenco, L., Schefer, S., Schuster, R., Tischler, M., and Ustaszewski, K.: The
780 Alpine-Carpathian-Dinaridic orogenic system: correlation and evolution of tectonic units, Swiss Journal of Geosciences, 101, 139-183, https://doi.org/10.1007/s00015-008-1247-3, 2008.

Stipčević, J., Tkalčić, H., Herak, M., Markušić, S., and Herak, D.: Crustal and uppermost mantle structure beneath the External Dinarides, Croatia, determined from teleseismic receiver functions, Geophysical Journal International, 185, 1103-1119, https://doi.org/10.1111/j.1365-246X.2011.05004.x, 2011.

785 Stipčević, J., Herak, M., Molinari, I., Dasović, I., Tkalčić, H., and Gosar, A.: Crustal Thickness Beneath the Dinarides and Surrounding Areas From Receiver Functions, Tectonics, 39, 15, https://doi.org/10.1029/2019TC005872, 2020.

Šumanovac, F.: Lithosphere structure at the contact of the Adriatic microplate and the Pannonian segment based on the gravity modelling, Tectonophysics, 485, 94-106, https://doi.org/10.1016/j.tecto.2009.12.005, 2010.

Tari, V.: Evolution of the northern and western Dinarides: a tectonostratigraphic approach. EGU Stephan Mueller Special
790 Publication Series, 1, 223-236. https://doi.org/10.5194/smsps-1-223-2002, 2002.

Tiberi, L., Costa, G., Rupnik, P .J., Cecić, I., and Suhadolc, P.: The 1895 Ljubljana earthquake: can the intensity data points discriminate which one of the nearby faults was the causative one?, Journal of Seismology, 22**,** 927-941, https://doi.org/10.1007/s10950-018-9743-z, 2018.

Ustaszewski, K., Kounov, A., Schmid, S. M., Schaltegger, U., Krenn, E., Frank, W., and Fügenschuh, B.: Evolution of the
795 Adria-Europe plate boundary in the northern Dinarides: From continent-continent collision to back-arc extension, Tectonics, 29**,** 34, https://doi.org/10.1029/2010TC002668, 2010.

Vičič, B., Aoudia, A., Javed, F., Foroutan, M., and Costa, G.: Geometry and mechanics of the active fault system in western Slovenia, Geophysical Journal International, 217**,** 1755-1766, https://doi.org/10.1093/gji/ggz118, 2019.

Vidrih, R. and Ribičič, M.: Potres 12. julija 2004 v zgornjem Posočju - preliminarne geološke in seizmološke značilnosti,
800 Geologija, 47(2), 199-220, 2004.

Vidrih, R., Sinčič, P., Tasič, I., Gosar, A., Godec, M., and Živčić, M.: Državna mreža potresnih opazovalnic = Seismic network of Slovenia, edited by: Vidrih, R., Environmental Agency of the Republic of Slovenia, Seismology and Geology office, 287 p, 2006.

Vignaroli, G., Faccenna, C., Jolivet, L., Piromallo, C., and Rossetti, F.: Subduction polarity reversal at the junction between
805 the Western Alps and the Northern Apennines, Italy, Tectonophysics, 450**,** 34-50, https://doi.org/10.1016/j.tecto.2007.12.012, 2008.

Zupančič, P., Cecić, I., Gosar, A., Placer, L., Poljak, M., and Živčić, M.: The earthquake of 12 April 1998 in the Krn Mountains (Upper Soča Valley, Slovenia) and its seismotectonic characteristics, Geologija, 44(1), 169-192, 2001.

Živčić, M., Bondar, I., and Panza, G. F.: Upper crustal velocity structure in Slovenia from Rayleigh wave dispersion, Pure
810 and Applied Geophysics, 157**,** 131-146, https://doi.org/10.1007/PL00001091, 2000.